Surrogate-based cyber-physical aerodynamic shape optimization of high-rise buildings using wind tunnel testing

Wei-Ting Lu[1], Brian M. Phillips[2*], and Zhaoshuo Jiang[3]

[1]Postdoctoral Associate, Department of Civil and Coastal Engineering,
University of Florida, Gainesville, United States

[2]Associate Professor, Department of Civil and Coastal Engineering,
University of Florida, Gainesville, United States

[3]Associate Professor, Department of Civil and Environmental Engineering,
San Francisco State University, San Francisco, United States

*Corresponding author, brian.phillips@essie.ufl.edu

Abstract

This study proposes a surrogate-based cyber-physical aerodynamic shape optimization (SB-CP-ASO) approach for high-rise buildings under wind loading. Three components are developed in the SB-CP-ASO procedure: (1) an adaptive subtractive manufacturing technique, (2) a high-throughput wind tunnel testing procedure, and (3) a flexible infilling strategy. The downtime of the procedure is minimized through a parallel manufacturing and testing (llM&T) technique. An unexplored double-section setback strategy with various cross-sections and transitions positions is used to demonstrate the performance of the proposed procedure. A total of 173 physical specimens were evaluated to reach the optimization convergence within the reserved testing window. Further analysis of promising shapes considering multiple design wind speeds is suggested to achieve target performance objectives at various hazard levels. Practical information on setback and cross-section modification strategies is discussed based on the optimization results. In comparison with a square benchmark model, the roof drifts for promising candidates with similar building volumes are reduced by more than 70% at wind speeds higher than 50 m/s. This procedure is expected to provide an efficient platform between owners, architects, and structural engineers to identify ideal candidates within a defined design space for real-world applications of high-rise buildings.

Keywords: Aerodynamic shape optimization, Surrogate modeling, Wind tunnel testing, CNC manufacturing, Tall buildings, Aerodynamic strategies

List of acronyms and notations

ASO	Aerodynamic shape optimization
BLWT	Boundary layer wind tunnel
CAD	Computer-aided design
CAM	Computer-aided manufacturing
CFD	Computational fluid dynamics
CNC	Computer numerical control
CP-ASO	Cyber-physical aerodynamic shape optimization
EI	Expected improved
FND	Farthest neighbor distance
HFFB	High-frequency force balance
KRL	KUKA Robot Language
IIM&T	Parallel manufacturing and testing
MSE	Mean square error
NHERI EF	Natural Hazards Engineering Research Infrastructure Experimental Facility
NMFP	Number of maximum feasible points
OTM	Overturning moment
PSD	Power spectral density
RPM	Revolutions per minute
SB-ASO	Surrogate-based aerodynamic shape optimization

SB-CP-ASO	Surrogate-based cyber-physical aerodynamic shape optimization
SQ	Square
TOPSIS	Technique for Order of Preference by Similarity to Ideal Solution
UF	University of Florida
$\overline{CMD}$	Mean along-wind base moment coefficient
RMS_{CML}	Root mean square across-wind coefficient
σ_{CML}	Standard deviation across-wind coefficient
B	The width of square section
B_F	Building width
d	The depth of side protrusion
f_1	Fundamental frequency
H_F	Building height
w	The width of side protrusion
ξ	Damping ratio

1. Introduction

It is well recognized that aerodynamic modification is an effective strategy to mitigate wind responses for high-rise buildings. The modification strategies can be divided into two categories: (1) cross-section modification and (2) height modification. The idea of cross-section modification is to alter flow characteristics, such as flow separation, flow attachments, or vortex shedding frequencies, by changing side (Lu et al., 2023) or corner geometries (Stathopoulos, 1985; Kwok et al., 1998; Kawai, 1998; Tamura and Miyagi, 1999; Gu and Quan, 2004; Tse et al., 2009; Tanaka et al., 2012; Carassale et al., 2014; Gu et al., 2020; Li et al., 2020). The concept of height modification is to destroy the coherence of vortex shedding in the across-wind direction by changing the cross-section at different elevations for a building. Methods include twisting (Tanaka et al., 2012; Li et al., 2021) , tapering (Tanaka et al., 2012; Chen et al., 2021; Li et al., 2022) , and setback (Kim and Kanda, 2010; Kim et al., 2011; Tanaka et al., 2012; Kim and Kanda, 2013). For the setback strategy, there is no study to systematically compare the aerodynamic behavior of high-rise buildings with different cross-sections at different elevations. For example, the ideal transition heights and ideal cross-sections at different elevations to mitigate wind responses is not clear. Thus, more information regarding on how to effectively utilize this strategy in real-world applications is needed. Due to the larger design space, however, it may not be feasible to find the answers using parametric study.

Instead, optimization is an efficient technique to seek ideal candidates in a large design space for an unknown problem with predefined objectives and constraints using limited resources. To find better solutions, potential candidates can be generated using traditional optimization strategies, such as particle swarm algorithms or genetic algorithms, and the outputs are evaluated immediately at each iteration until a stop criterion is activated. Valid solutions are returned anytime along the iteration before the results are converged. For problems that consist of continuous variables, such as shape optimization, it is expected that there is a correlation in behavior between adjacent solutions. This characteristic can be leveraged using the surrogate modeling technique (Jones et al., 1998; Forrester and Keane, 2009; Ahmed et al., 2009) to predict the behavior of the entire search space with limited data points. To increase the accuracy of surrogate modeling, an adaptive infilling strategy based on the latest collected information can be used to achieve the goal of optimization. This technique is called surrogate-based (or model-based) optimization procedure. In comparison with the traditional optimization strategies, this is a more efficient technique for problems with large search space. The surrogate-based aerodynamic shape optimization (SB-ASO) procedure has been successfully applied to different wind-sensitive structures in civil engineering, including bridge decks (Xu et al., 2020), large-span structures (Qiu et al., 2022), low-rise buildings (Townsend et al., 2023), and high-rise buildings (Bernardini et al., 2015; Elshaer et al., 2017; Ding and Kareem, 2018; Elshaer and Bitsuamlak, 2018; Paul and Dalui, 2021; Wang et al., 2022; Wang et al., 2023) using computational fluid dynamics (CFD) or offline wind tunnel testing data.

For high-rise buildings, however, CFD simulation is not able to accurately capture the flow characteristics around a bluff body immersed in the boundary layer effects (Bernardini et al., 2015), in particular when deviating from classical benchmark shapes. According to ASCE 7-22, conducting wind tunnel testing is required to obtain the design demands for tall buildings which are not with regular external shapes. Since uniqueness is an important design objective, it is reasonable to say that wind tunnel testing is needed for all high-rise buildings for real-world applications. However, there is currently no study to integrate a SB-ASO procedure with physical testing, meaning that only limited candidates are evaluated in the wind tunnel at the preliminary design stage.

Fig. 1 (a) shows an iterative traditional cyber-physical aerodynamic shape optimization (CP-ASO) procedure, which involves three components: model manufacturing, model testing, and an optimization algorithm. The cyber component can be a traditional or surrogate-based optimization algorithm. In the iterative process, the new data point for manufacturing and testing is unknown until the latest results are obtained. This implies that model manufacturing plays a crucial role on the efficiency of the entire procedure since the testing cannot be carried out until the model is produced, which is a major difference for optimization problems using physical testing. The issue of manufacturing can be relieved if a new testing candidate can be rapidly changed via adaptive mechanical devices, such as the height of parapet wall of a low-rise building (Whiteman et al., 2018), the fundamental frequencies of a high-rise building (Fernandez-Caban et al., 2020), and the angles of a fin system for a high-rise building (Whiteman et al., 2022). However, only changes within the mechanical range of motion can be achieved using mechatronic models, implying that the dimensionality/complexity of the search space is limited due to physical constraints.

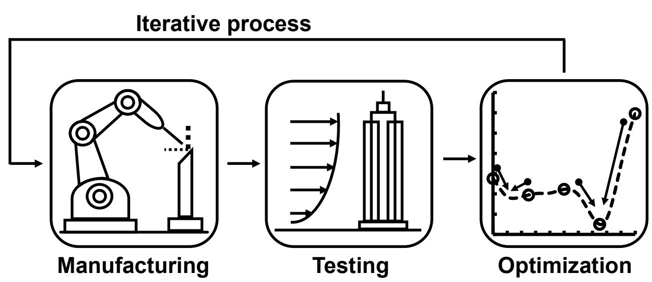

(a) Sequential procedure

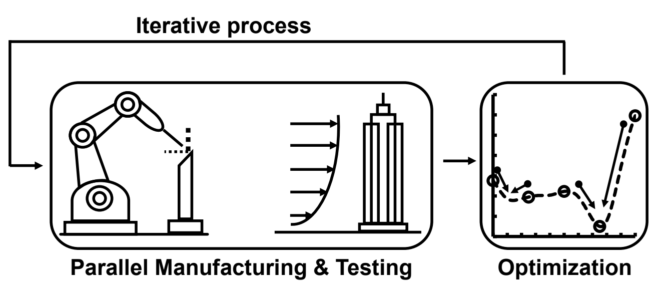

(b) The procedure with IIM&T proposed in this study

Fig. 1. Conceptual procedure for CP-ASO procedure

For SB-ASO, there are several types of surrogate models available in the literature, including kriging, radial basis function, support vector regression, artificial neural network, etc. Among these surrogate models, kriging is a Gaussian process interpolation technique that can predict outputs based on the distances and variations between collected data points (Krige, 1951; Matheron, 1963; Sacks et al., 1989). Although there are variations of kriging, ordinary kriging is the most common model type used by several studies (e.g., Bernardini et al., 2015; Xu et al., 2020; Qiu et al. 2022) because it is easy to select model parameters. In ordinary kriging, users only need to determine the type of regression model and the range of the corresponding hyperparameter.

In addition, kriging is able to provide the predicted mean square errors (MSEs) in the design space, which is a promising indicator for adaptive infilling since all collected data points can be used for updating the surrogate model. An MSE-based infill strategy can be used to increase the global accuracy of surrogate modeling by infilling new data points with the largest predicted MSE. For optimization purposes, after an acceptable level of global accuracy is achieved, the second stage is to infill/validate the predicted optimum if it has not been collected. For an unexplored problem, however, it may not be easy to evaluate the global accuracy of a surrogate, meaning that it is hard to define the stop criterion for the MSE-based approach in the two-stage optimization process. Exhaustive global exploration will waste resources, while insufficient global exploration will result in becoming trapped at local optimal solutions. Since the surrogate model continues to be updated in the second stage, it is also not clear how many points need to be infilled for optimum validation (optimization) purpose. Other than the MSE, the expected improved (EI) is another popular infilling strategy to increase the local accuracy of surrogate models by directly including the objective function when making infilling decisions. However, this approach can easily get stuck at a local optimum if a certain level of global accuracy is not achieved (Forrester and Keane, 2009), meaning that EI is not a flexible approach for optimization.

Other than the robustness of the infilling strategy discussed above, there are other considerations that need to be addressed when it comes to CP-ASO using the surrogate model technique. First, in general, wind tunnel testing windows are reserved in advance, meaning that the optimization process needs to converge within a fixed time. Although a stop criterion based on time, such as total iteration, can be applied, it is preferred to achieve a balance between global exploration of the search space and convergence to the optimization results by fully utilizing the entire testing window (not to stop too early). Second, the CP-ASO procedure is using a physical resource and may be interrupted. The ability to return valid optimum solutions anytime along the iteration process is preferred, which is not be able to achieve using either the MSE or EI strategies because data points are not infilled at predicted optima. Third, the results of physical testing are nondeterministic. The infilling strategy must include features to address experimental uncertainty and also flag potential outliers. With the aforementioned considerations, there is a need to develop a tailored infilling strategy for the CP-ASO procedure using the surrogate-based technique.

This study proposes a surrogate-based cyber-physical aerodynamic shape optimization (SB-CP-ASO) procedure for high-rise buildings. The procedure consists of three components with techniques to overcome the aforementioned challenges, as shown in Fig. 1 (b). In the physical part, an adaptive subtractive manufacturing technique, which is able to produce complex external shapes for high-rise buildings, and a high-throughput high-frequency force balance (HFFB) wind tunnel testing procedure are developed at the University of Florida (UF) Boundary Layer Wind Tunnel (BLWT). In the cyber part, a robust infilling strategy augmented with surrogate-based local search is proposed to pursue a balance between global exploration and optimization. The infilling strategy is able to: (1) return valid optimal solutions anytime in the iteration, (2) ensure the local accuracy at promising regions, and (3) escape a local optimal solution. A parallel manufacturing and testing (llM&T) technique is realized by an indicator, “sparsity level”, to integrate the three components together with the intention of maximizing the throughput of the procedure. A double-section setback shape optimization problem for high-rise buildings with three design variables is used to demonstrate the robustness of the proposed procedure. Practical information is provided regarding ideal transition position of the setback strategy with different cross-sections.

This paper is organized as follows. Section 2 discusses some unique considerations for shape optimization design of high-rise buildings. The three components and llM&T in the SB-CP-ASO procedure are introduced in Section 3. The optimization problem and the setup of the SB-CP-ASO procedure are presented in Section 4. The reliability of the three components and optimization results are discussed in Section 5. The selection approach of promising candidates for high-rise buildings considering multiple design wind speeds is presented in Section 6 with the conclusions summarized in Section 7.

2. Background

To conduct wind design for high-rise buildings, both the time and frequency domain results are needed to calculate the structural responses (e.g., base overturning moment, roof drift, and roof acceleration) under different wind speeds and wind angles (ASCE 7-22, 2022). Due to the variation of power spectral density (PSD) responses in the frequency domain results, the structural responses do not change linearly with wind speed. When aerodynamic strategies are compared, the relative performance between different candidates varies with the design wind speed (Lu et al., 2023). This indicates that different cities will have different optimal solutions given the same optimization problem. Additionally, a promising candidate is expected to achieve multiple aerodynamic performance objectives, such as serviceability and survivability at different hazard levels (Kareem, 1983; Irwin, 2009).

Due to the complex behavior mentioned above, it may not be practical to use the structural response or frequency domain results as an objective function for the optimization process. Thus, statistics from time domain results are used as objectives functions to find optimal candidates for SB-ASO problems of high-rise buildings (Bernardini et al., 2015; Elshaer et al., 2017; Ding and Kareem, 2018; Elshaer and Bitsuamlak, 2018, Paul and Dalui, 2021). However, the link between structural responses under different design wind speeds and the time domain results were not addressed in the literature. The appropriateness of using time-domain statistics for surrogate modeling and optimization in achieving excellent structural scale responses for high-rise buildings is needed.

In addition to aerodynamic performance, other design considerations, such as aesthetic appeal, building volume, and operation purposes, also influence the external shape of a high-rise building. Therefore, seeking a single solution with the best aerodynamic performance is not enough for owners and architects at the preliminary design stage. Instead, a group of candidates which can satisfy a defined threshold is required for designers to have more freedoms to achieve different objectives, a practical consideration of ASO procedure for high-rise building design.

This section discussed some unique aspects of optimization design for high-rise buildings which are not addressed in the literature. A customized approach to identify a set of ideal candidates under multiple design wind speeds for high-rise buildings will be introduced along the optimization results in Section 6.

3. SB-CP-ASO procedure

The proposed SB-CP-ASO procedure is illustrated in Fig. 2 (a). The procedure includes the following three components: (1) an adaptive milling manufacturing procedure, discussed in Section 3-1, (2) a high-throughput wind tunnel testing procedure, discussed in Section 3-2, and (3) a flexible infilling strategy, discussed in Section 3-3. The procedure begins by selecting an initial set of samples within the design space. The ideal number of initial samples is problem dependent. It can be determined based on the number of models that can be evaluated in the testing window or the number of feasible models in the search space. These samples are then fabricated and evaluated in the wind tunnel. An initial kriging surrogate model is constructed after the results of the initial samples are collected. From that point onward, the kriging model is used as part of the infilling strategy to suggest the next sample to manufacture and evaluate in the wind tunnel. After each testing, the kriging model is updated and the process repeats. The iterative process is continued until one of the two established stop criteria for the infill strategy is activated. The first stop criterion is the total allowable duration of the tests, a practical limitation for a shared resource such as a wind tunnel. The second criterion is flexible and controlled by the optimization strategy, which will be discussed later (Section 3.3.3). Ideally, the stop criterion is activated by the optimization strategy, meaning the optimization results are converged.

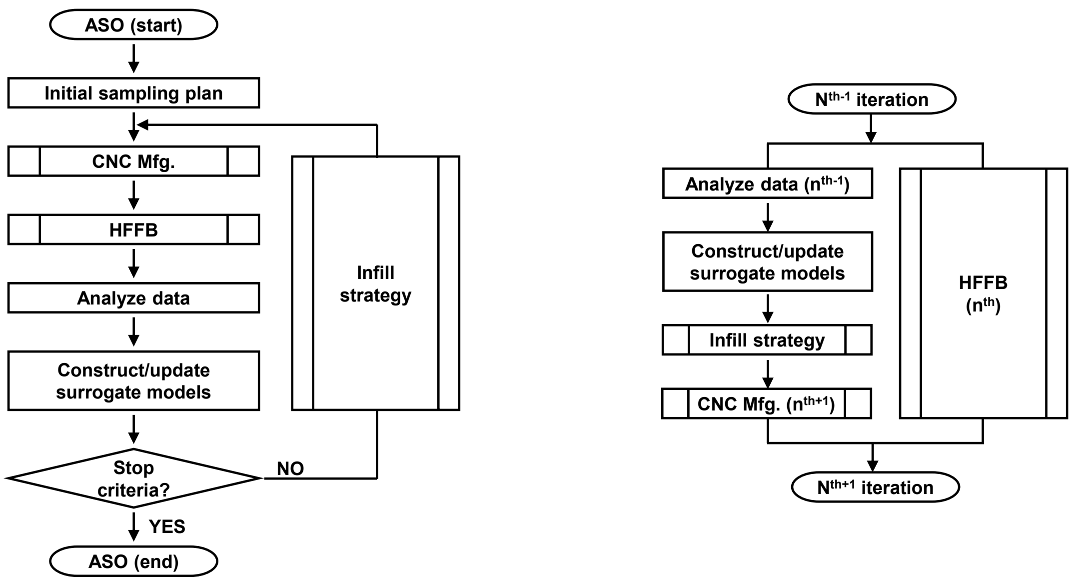

(a) The procedure for n^{th} model (b) The concept of IIM&T at n^{th} iteraiton

Fig. 2. SB-CP-ASO procedure.

As shown in Fig. 2(a), the efficiency of the procedure will be significant reduced if the manufacturing and testing are in series for shape optimization problems with major modifications. To address this issue, the IIM&T is proposed to let the three components be conducted at the same time, as shown in Fig. 2 (b). It should be pointed out that Fig. 2 (a) and (b) do not conflict with each other, but are illustrated from different perspectives, which are from the n^{th} model (Fig. 2 (a)) and n^{th} iteration (Fig. 2 (b)). The concept of IIM&T is to manufacture the n^{th+1} model based on the available information from cyber part (analyzing testing results, updating the surrogate model, and running the infilling strategy) when the n^{th} model is tested in the wind tunnel. At each iteration, the downtime can be minimized if the summation of the time for cyber part and physical manufacturing is shorter than the time for physical testing. More details regarding how to realize this technique will be discussed in Section 3-3.

3.1 Adaptive subtractive manufacturing procedure

Milling (subtractive manufacturing) is a process to manufacture a target shape by removing material from an initial workpiece. This manufacturing process can be achieved using computer numerical control (CNC) technique in which the movement of milling tools is operated via pre-programmed numerical control. Multi-axis industrial robotic arms are recognized as a promising tool for CNC milling manufacturing because of their high flexibility and large workspace. A 6-axis industrial robotic arm (KUKA model KR 20 R1810-2) was used to manufacture different models for this study, as shown in Fig. 3. A 3 hp 18,000 rpm ATI Model SC30 spindle with automatic tool changer was installed on the robot to control various flat and ball end mills for CNC milling (see Fig. 3 (a)). A turntable 50 cm away from the base of the robot was installed to provide an additional axis (7^{th} axis) to increase the workspace of the system (see Fig. 3 (b) and (c)). A 5C collet chuck was installed on the turntable to hold a model for CNC milling (see Fig. 4 (a)).

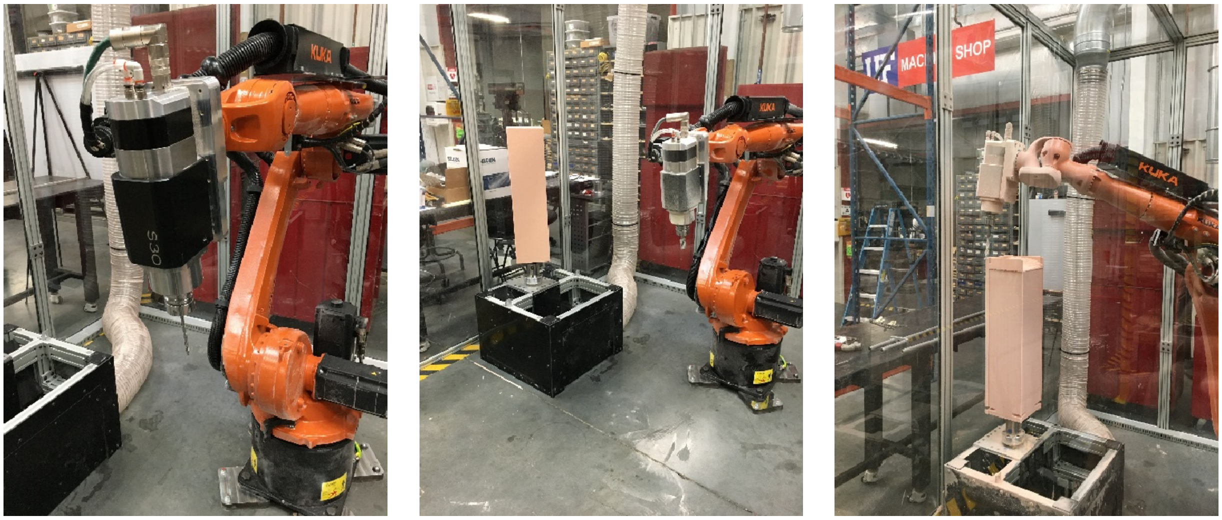

(a) (b) (c)

Fig. 3. Photographs for the adaptive CNC subtractive procedure.

Blocks of urethane foam material with a density of 96 kg/m^3 and a hardness of 8 Shore D on the Durometer scale were used to fabricate the models for wind tunnel testing. All model blanks began as a square prism 90 mm x 90 mm in plan and 405 mm in height as shown in Fig. 4 (a). For a consistent base size for wind tunnel testing, all models included a 5 mm thick, 90 mm x 90 mm square base. The top of this base was set flush with the wind tunnel floor. A 25.4 mm outer diameter hollow aluminum rod with 3.175 mm wall thickness was inserted in the model to provide sufficient stiffness to avoid interactions between the upper bound of the frequencies of interest and specimen's fundamental natural frequency under wind excitation. An 85 mm x 85 mm in plan 10 mm thick 3D-printed collar was clamped to the aluminum rod and glued to the bottom of the model to provide torsional resistance between the rod and the model. Fig. 4 (b) shows the aluminum rod with the plastic collar. The rod and collar are reusable for a new foam blank.

(a) Blank model in the 5C collect chuck. (b) Aluminum rod with plastic collar. (c) Plate with the notch.

Fig. 4. Photographs of details for foam model.

The adaptive CNC subtractive manufacturing procedure is realized by a remanufacturing technique to reuse previously tested foam models, saving time and material. The procedure of the adaptive CNC manufacturing is illustrated in Fig. 5 (a). On the software side, an algorithm was developed to select from among a set of available, previously tested models. The previously tested models that the new target model can nest into are considered. Milling volumes are calculated based on the difference between the target model and the tested models. The zig-zag cutter path strategy, equidistant parallel lines that fit within the milling volumes, is adopted in this study to avoid redundant tool paths and to minimize manufacturing time. Parametric design for different CNC coordinate milling paths is developed using C# scripts to interface with computer-aided design/manufacturing (CAD/CAM) software Rhino6 and Grasshopper. A plug-in KUKAprc is used to convert the tool paths into KUKA Robot Language (KRL). If there is more than one feasible candidate, reusability and the predicted manufacturing time are used as selection criteria to prioritize the models. If there are no suitable models available to reuse, a blank model (see Fig. 4 (a)) will be used to make the target model. On the hardware side, a 1 cm long notch is included at the end of all aluminum rods (see Fig. 4 (b)). A plate with the same notch, as shown in Fig. 4 (c), was installed at the bottom of the 5C collet chuck to ensure that a previously tested model can be reinstalled at the same elevation and orientation in the 5C chuck for remanufacturing.

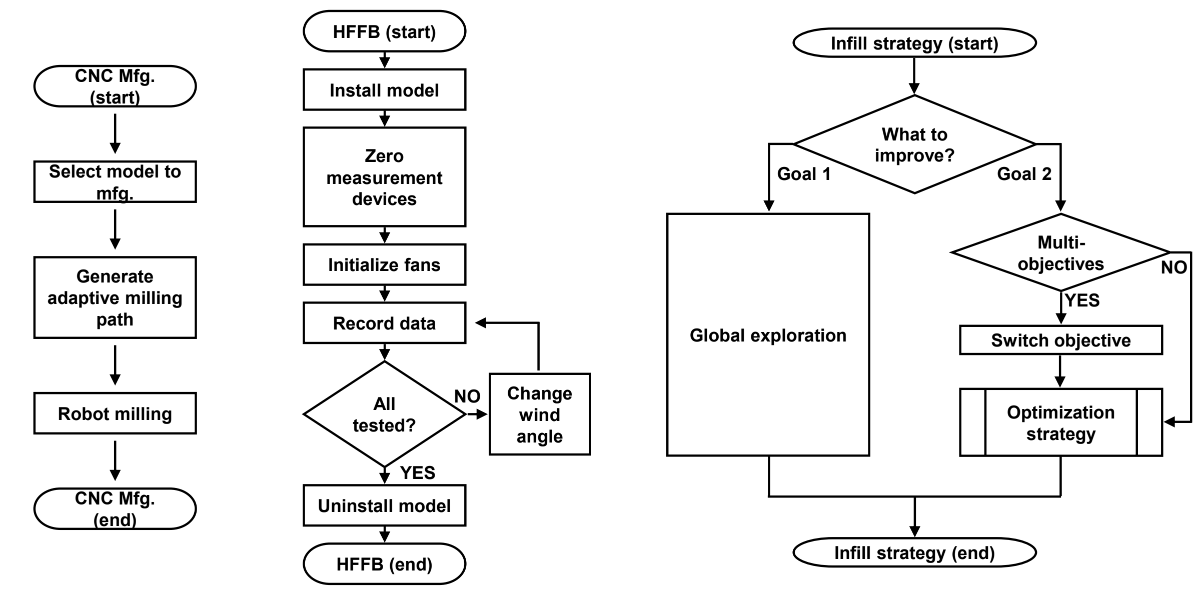

(a) CNC procedure (b) HFFB testing procedure (c) Infilling strategy

Fig. 5. Procedures for tasks described in Section 3.

3.2 HFFB testing procedure and evaluation approach

A high-throughput HFFB BLWT testing procedure (Fig. 5 (b)) is established at the UF NHERI EF (Natural Hazards Engineering Research Infrastructure Experimental Facility) to accurately capture the base responses of different testing candidates with complex external shapes. The base responses (e.g., overturning moments, OTM) can be used to generate structural responses (e.g., roof drift) of interest (Tschanz and Davenport, 1983; Zhou et al., 2003; Kwon et al., 2008). The Terraformer, an automated roughness grid composed of 1116 elements, was used to generate desired approach flow conditions in the test section. More details of the UF BLWT can be found in literature (Catarelli et al., 2020a; Catarelli et al., 2020b). In addition to approach flow conditions, wind angle is another important testing condition for high-rise buildings (ASCE 7-22, 2022). The desired wind directions were realized by an automatic turntable in the wind tunnel. During testing, a TFI cobra probe was installed at the model height offset in the spanwise direction to capture the reference wind speed.

The high-throughput testing procedure is supported by a fast installation mechanism for the models. The installation mechanism is shown in Fig. 6. A 5C collet chuck, which is identical to the chuck for manufacturing, was installed on a six-axis load cell (ATI Industrial Automation, Delta model) to hold the models as shown in Fig. 6 (a). The load cell was used to measure the base reactions during HFFB BLWT testing. On the wind tunnel floor, a wood panel with a 96 mm x 96 mm square opening was made to fit the base (90 mm x 90 mm square) for all testing models. A 180 mm x 180 mm square opening provides access to the collet chuck nut for changing models (see Fig. 6 (b)). This panel was closed during testing (see Fig. 6 (c)). With this setup, the models can be installed quickly and at a consistent elevation and orientation. As shown in Fig. 5 (b), the load cell and cobra probe were zeroed after model installation and prior to engaging the fans.

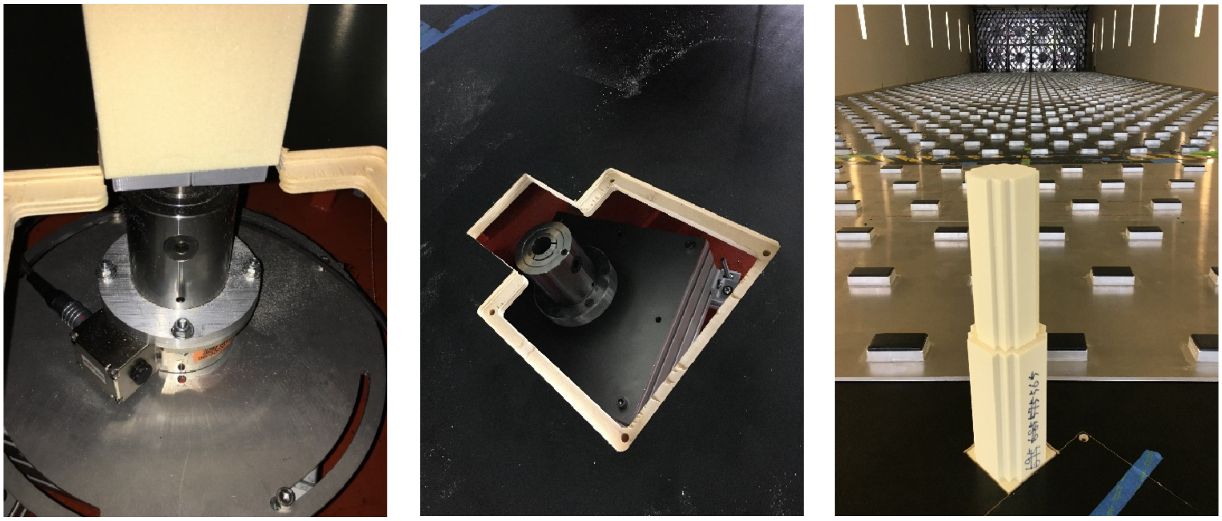

(a) Close view (b) Wood panel (c) During testing

Fig. 6. The setup of load cell and 5C collect chuck in the wind tunnel.

In this study, the time series results of base moments were used to assess the aerodynamic performance for each model. As mentioned in Section 2, both the time domain and frequency domain results in different wind angles are needed to generate the structural responses for high-rise buildings. In the time domain, the non-dimensional base coefficients (mean, root mean square, and standard deviation) for each wind angle were calculated. The PSD curves for each wind angle were calculated from the frequency domain responses. The statistical time domain responses and PSD responses were enveloped across all wind angles to generate full-scale OTM responses at different wind speeds assuming a Gaussian process. The structural responses were calculated using a modal analysis procedure (Zhou et al., 2003; Kwon et al., 2008). More details on this HFFB post-processing approach can be found in the literature (Lu et al., 2023).

3.3 Infilling strategy

For continuous problems, parameter discretization is a crucial step to achieve an economical and effective optimization process. If the discretization interval is too large, a critical design alternative might be missed. If the interval is too small, the results might be insensitive to the incremental changes of inputs, leading to redundant samples and wasted resources. For physical testing, furthermore, the difference in results between neighboring samples may be dominated by experimental uncertainty rather than the small interval of input parameters, complicating the optimization process and surrogate modeling. Thus, appropriately selecting intervals for the design parameters is an important step for the infilling strategy.

The flow chart of the infilling strategy is shown in Fig. 5 (c). There are two goals for the infilling strategy: (Goal 1) improving the global accuracy of surrogate modeling, and (Goal 2) seeking the optimum solution for an objection function. In this study wind, tunnel testing controls the throughput, so only one data point is infilled at each iteration. As mentioned in Section 1, it is not easy to evaluate the global accuracy for an unexplored surrogate model problem. Instead of adopting a decoupled strategy where the surrogate model is fully trained and then used to evaluate the optimal solution, a switch between the two infilling goals along the SB-CP-ASO procedure is proposed in this study. There are two benefits for the switch between the two infill goals. First, the ASO procedure can return a set of valid optimum solutions anytime in the case that the physical testing must be halted prematurely. Second, it naturally introduces a jump-out mechanism into the optimization process.

The infill ratio and conditional operation between the two infill goals can be defined by the user. A larger infill ratio on global exploration leads to a better understanding of the entire design space but more iterations will be needed to achieve the convergence of the procedure. In contrast, if the infill ratio on optimization is higher, the solution will converge more quickly, but the chance of getting stuck at a local optimum is increased. The operator that selects between the two infill goals can be fixed or evolve based on the iteration count or results themselves. In addition to single objective, the procedure is also able to pursue multiple objectives in parallel as needed, as shown in Fig. 5 (c). It is suggested to switch the optimization objectives in a fixed sequence at each iteration.

3.3.1 Sparsity level for IIM&T

As shown in Fig. 2 (b), the idea of IIM&T is to manufacture the n^{th+1} model when the n^{th} model is tested in the wind tunnel. Since the output for the n^{th} model is unknown, the sparsity level is proposed in the infilling strategy to consider the position (input) in the design space of the 1^{st} to the n^{th-1} previously tested models and the n^{th} model in the wind tunnel. With parameter discretization, there are finite data points that can be infilled in the design space. The sparsity level is defined as the ratio between the number of uncollected points and the number of maximum feasible points (NMFP) that can be infilled within the farthest neighbor distance (FND) for a point of interest. The FND is defined as:

$$FND = \sqrt{D * d^2} \tag{1}$$

where D is the dimensionality of the problem and d is the normalized unit-distance in the design space. The concept of sparsity level is illustrated in Fig. 7 using a 2D example. The unit distance is 1 for both variables and the corresponding FND is 1.4-unit distance.

For Point A, the NMFP is 8 and there are 7 uncollected points, which can be infilled within the FND. The corresponding sparsity level for Point A is 87.5% (=7/8). The sparsity levels for Point B and Point C are 67% (=2/3) and 60% (=3/5), respectively. Because the sparsity level is normalized by the NMFP, it fairly evaluates points on the vertexes, edges, and interior of the design space.

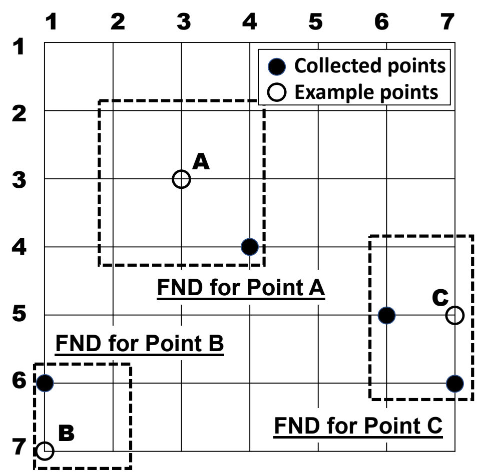

Fig. 7. The concept of sparsity level.

3.3.2 Infill Goal 1: Global exploration

For infill Goal 1, the predicted MSE (from kriging) and sparsity level (Section 3.3.1) are considered when selecting the infilling point. Both the collected information of input and output is used to generate the predicted MSEs for all uncollected points except for the model in the wind tunnel. The inputs for all tested models and the current model in the wind tunnel are used to calculate the sparsity level. The technique for order of preference by similarity to ideal solution (TOPSIS, (Hwang et al., 1981; Yoon, 1987; Hwang et al., 1993)) is used to calculate the scores using the predicted MSE and sparsity level for all candidate points (uncollected points excluding the model in the wind tunnel) at each iteration. The point with the highest score from the TOPSIS is selected for the infilling point and manufacturing.

In general, the predicted MSEs are proportional to the distance between predicted points and collected points. If collected points are sparse at a region, the corresponding predicted MSEs for the uncollected points will be relatively high in the region. Sparsity level is proposed to realize the IIM&T technique by compensating for the unknown outputs of the model currently in the wind tunnel. If the sparsity level is not adopted, the suggested infill point will cluster together with the model currently in the wind tunnel due to the high predicted MSE, resulting in redundant exploration. On the other hand, the sparsity level alone is insufficient because most uncollected points will have the same sparsity score of 100%. To balance the two criteria, it is suggested to use equal weight ratios for the sparsity level and the predicted MSE to ensure the effectiveness of the IIM&T technique.

3.3.3 Infill Goal 2: optimization

The procedure of the infill strategy for optimization is illustrated in Fig. 8. The first step is to determine the predicted optimal solution from the most up-to-date surrogate model. There are only two situations for the predicted optimal solution as illustrated in Fig. 9 using a 1D example. For Situation (a), the predicted optimum is better than the best observation (see Fig. 9 (a)). Situation (a) represents that the predicted optimum has not been collected. As mentioned in Section 1, wind tunnel testing is required when evaluating wind loads high-rise buildings with irregular shapes. This implies that promising aerodynamic shapes should be evaluated in the wind tunnel. By infilling a data point at the predicted optimum ("optimum validation" as shown in Fig. 8), the concern of an inaccurate prediction is relieved. For Situation (b), the surrogate model's predicted optimum has already been gathered via wind tunnel testing (see Fig. 9 (b)). For this situation, a surrogate-based local search strategy will be executed with infilling to: (1) seek a better neighboring solution, and (2) ensure the local accuracy around the predicted optimum.

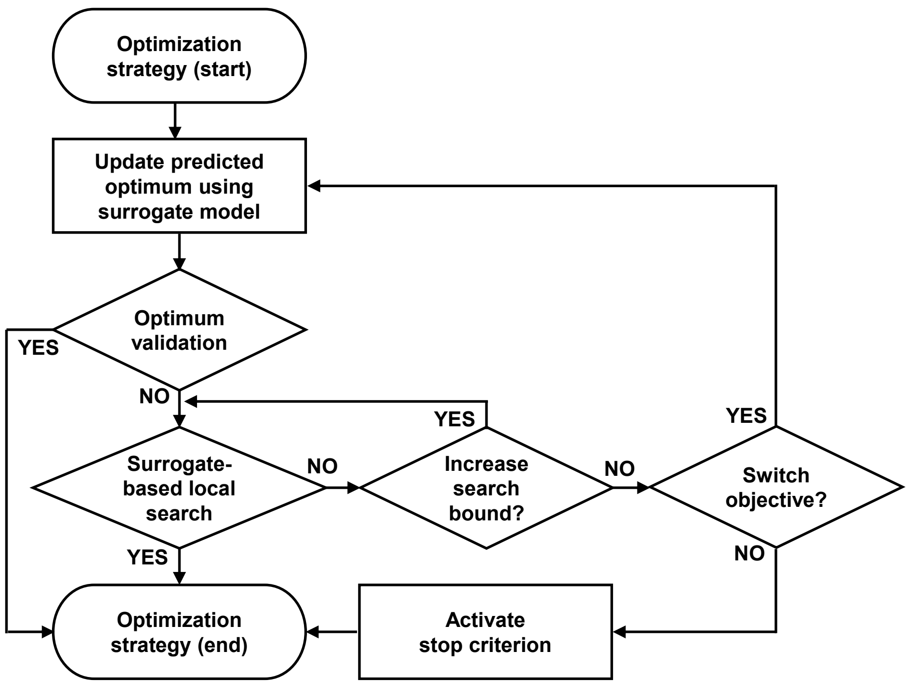

Fig. 8. Selecting an infill point based on optimization.

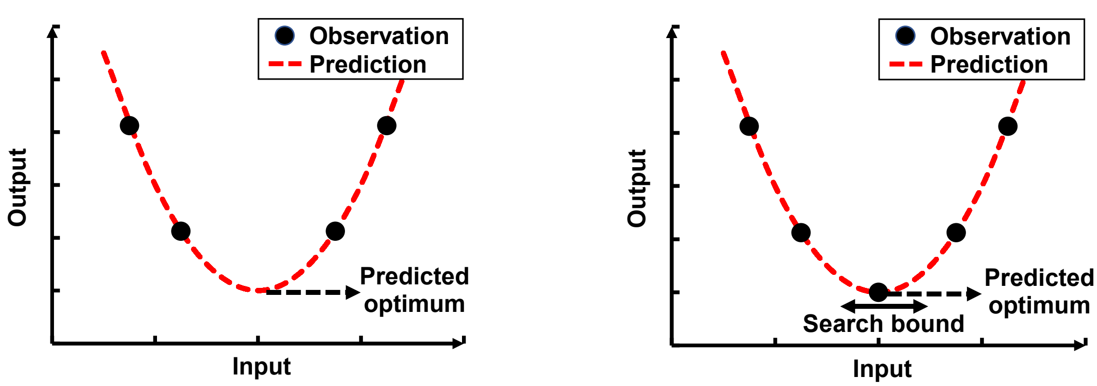

(a) Optimum validation (b) Surrogate-based local search

Fig. 9. The two situations for optimization infilling

The idea of the surrogate-based local search is to infill an uncollected data point with the largest predicted MSE within a defined search bound, as shown in Fig. 10. The search bound is centered on the predicted optimum/best observation (e.g., Point A (3,3), see Fig. 10). The radius of the search bound ranges from the discrete distance of 1-unit distance to the FND of the search space (e.g., 1.4-unit distance for 2D problem), which is related to the convergence speed of the optimization process. With parameter discretization, the numbers of points that can be infilled in Fig. 10 for 1-unit and 1.4-unit distance are 4 points and 8 points, respectively. For a large search bound (e.g., 1.4-unit distance), although there are more data points (8 points) that need to be infilled to reach convergence, the chance to achieve a better solution using fewer overall iterations increases. The reason behind this is because the uncollected points (Point (2,2), Point (2,4), Point (4,2), and Point (4,4)) with the greatest distance from the center of the search bound have a higher chance to be infilled first due to the larger predicted MSE. If a better solution occurs at one of these points, several intermediate iterations can be avoided in comparison with using 1-unit distance as the search bound. Since the optimum prediction is updated at every iteration, the center of the search bound might move along the iteration. If the predicted optimum/best observation remains the same and all points within the search bound are all collected, then that objective is considered converged.

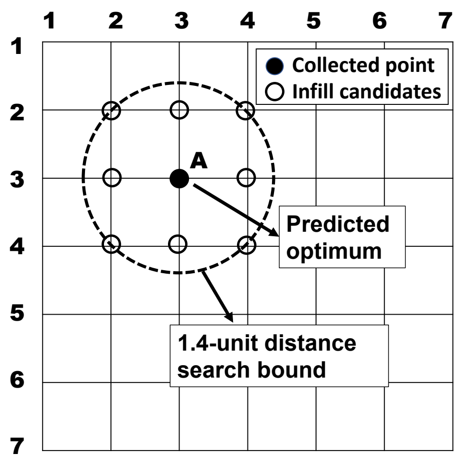

Fig. 10. The concept of surrogate-based local search

In general, the ideal size of the local search bound is problem-dependent. Instead of a fixed local search bound, an adaptive local search bound along the iteration process is proposed in this study. A small local search bound can be taken as a starting point. For single-objective case, if the results are converged early in the reserved testing window, the procedure can be continued by increasing the size of the local search bound. If the local search bound is full and not increased, the stop criterion of the optimization process will be activated (see Fig. 8). With the adaptive search strategy, the entire testing window is expected to be fully utilized since stop criterion is controlled by users.

For the multi-objective case, each objective is fit using its own independent surrogate model. As a new point is infilled, all surrogate models are updated in parallel. In other words, infilling for one objective will improve the surrogate modeling of all objectives at that infill point. By doing this, seeking a better optimal solution for one objective can benefit to the global accuracy or the optimal solutions for other objectives. If an objective is converged, then either: (1) the search bound can be increased for the objective, or (2) the algorithm can switch to another optimization objective at this iteration (see Fig. 8). Note that it is possible to discover a better solution from the jump-out mechanism, even for objectives that had been considered converged. For this reason, it is suggested to increase the search bounds for different objectives at the same time.

3.3.4 Summary of infilling strategy

As mentioned in Section 1, the issues of the two-stage infilling strategy of MSE and optimal validation are (1) not easy to define a stop criterion between the two strategies, and (2) easy to get trapped at a local optimal solution with insufficient global exploration. By switching the two infilling strategies, the first issue disappears and the second issue is partially resolved. In addition to find a better solution, the surrogate-based local search algorithm is able to further relieve the second issue by improving the local accuracy of promising region when the surrogate model suggests the same optimal solution. The benefits of improving local accuracy are to (1) find similar promising solutions within the search bound, which provide important information for architectural considerations (see Section 2), and (2) eliminate the concerns of uncertainties from physical testing based on the trends of the results in the local search bound. The two benefits cannot be achieved using the global exploration goal, meaning that the proposed surrogate-based local search optimization procedure is a practical step for SB-CP-ASO problems of high-rise buildings.

4. Optimization problem and the setup of the SB-CP-ASO procedure

A double-section setback building with three design variables is selected as an example to demonstrate the robustness of the proposed ASO procedure. The elevation view of the problem is presented in Fig. 11(a). The total model height is fixed at 40 cm. Input#1 and Input#2 are the widths of side protrusions on the top and bottom sections, respectively (Fig. 11(b)). Input#3 is the transition position between the two sections. The top and bottom sections can each independently be described by the designation SQ B-d-w, as shown in Fig. 11 (b), where SQ represents the square section, B is the dimension of the square, d is the depth of side protrusion, and w is the width of side protrusion. B and d are fixed for each of the two sections, resulting in one parameter w for each section. In this study, the depth ratio is defined as the ratio between d and B and the width ratio is defined as the ratio between w and B.

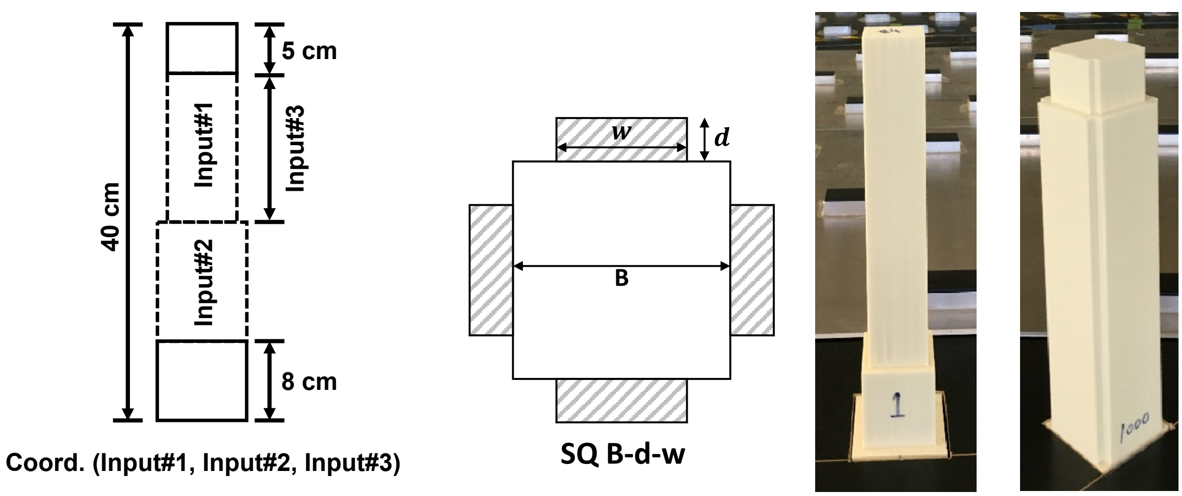

(a) Elevation view (b) Cross-section (c) (1,1,1) (d) (10,10,10)

Fig. 11. Illustration of the optimization problem with 3 inputs.

The design space is discretized into 10 options for each input. Discrete options for Input#1 and Input#2 are shown in Fig. 12 and Fig. 13, respectively. The depth ratios, which are fixed, for the top and bottom sections are 12.5% (7 mm) and 14.3% (10 mm), respectively. The width ratios, which are the design variable for both sections, vary from 0% to 100%. The smallest intervals of side protrusion width for the top and bottom sections are 6 mm and 8 mm, respectively, which are equivalent to a 10% modification ratio with respect to the square section. Based on the literature (Stathopoulos, 1985; Kwok et al., 1998; Kawai, 1998; Tamura and Miyagi, 1999; Gu and Quan, 2004; Tse et al., 2009; Tanaka et al., 2012; Carassale et al., 2014; Gu et al., 2020; Li et al., 2020; Lu et al., 2023), these intervals are sufficient to produce different aerodynamic responses (i.e., detectable above experimental uncertainty). It can be observed that the top section can always nest into the bottom section, ensuring that any combination of the two features will result in a realistic building. Table 1 lists the transition positions for Input#3 with an interval of 30 mm (7.5% of model height). The lowest and highest transition positions are 80 mm (20% of model height) and 350 mm (87.5% of model height), respectively from the ground.

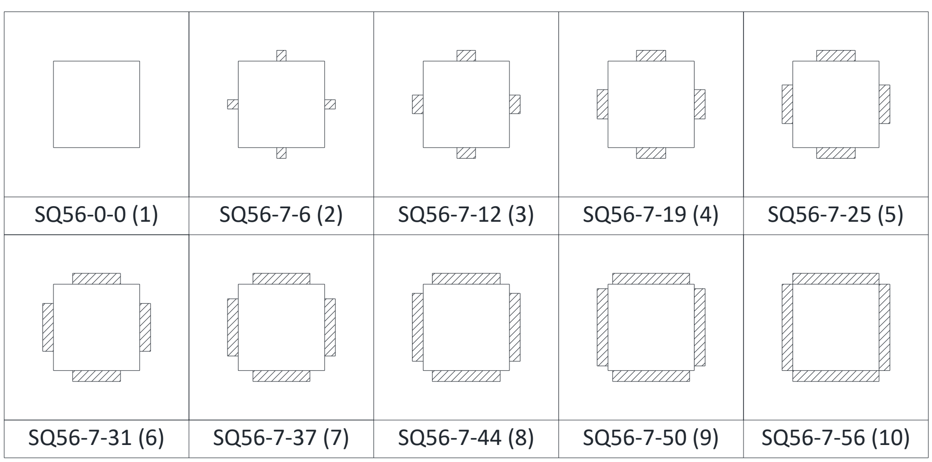

Fig. 12. Plan view and detail for the top section (Input#1). The numbers in the parentheses indicate the corresponding coordinates in the optimization problem.

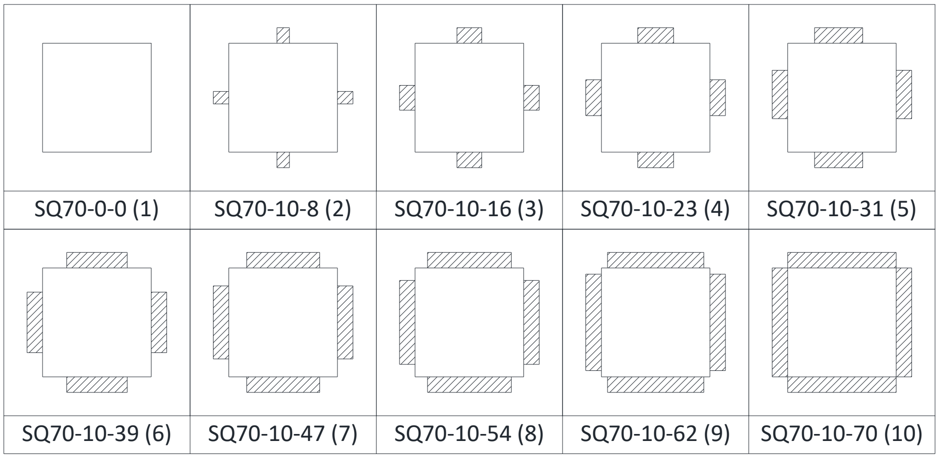

Fig. 13. Plan view and detail for the bottom section (Input#2). The numbers in the parentheses indicate the corresponding coordinates in the optimization problem.

Table 1. The transition positions for input#3.

Option	Transition height (mm)	Percentage of bottom section (%)
1	80	20%
2	110	27.5%
3	140	35%
4	170	42.5%
5	200	50%
6	230	57.5%
7	260	65%
8	290	72.5%
9	320	80%
10	350	87.5%

With the selected parameter discretization, there are 1000 feasible candidates, which cannot feasibly be explored using an exhaustive search approach through wind tunnel testing. Each candidate can be represented using coordinates (Input#1, Input#2, Input#3) with a range of [1,10] in the search space. Among the candidates, the max (10,10,10) and minimum (1,1,1) building volumes are 2930 cm^2 and 1397 cm^2, respectively (see Fig. 11 (c) and (d)). A prismatic square model (70 mm x 70 mm, SQ70) with a volume of 1960 cm^2, which is in the middle of the search space, is taken as the benchmark to validate the wind tunnel testing conditions and to demonstrate the benefits of the setback strategy. Although the range of the building volume is significant in the design space, the solutions with ideal aerodynamic performance are not expected to occur at the extreme model volumes. In addition, as mentioned in Section 2, there are other factors need to take into consideration when it comes to design a high-rise building, such as operation purpose, construction cost, and return on investment, etc. The aerodynamic performance of the models with extreme building volumes can provide useful references for designers to evaluate optimal candidates in the preliminary design stage.

4.1 The setup of the adaptive subtractive manufacturing procedure

As mentioned in Section 3, previously tested models will be reused in the ASO procedure to the extent possible to save material cost and manufacturing time. There were 50 pairs of rods and collars (see Fig. 4 (b)) created to support a maximum of 50 models at the same time in the lab. A maximum of 40 tested models were preserved for reuse alongside ten blanks. If there were more than 40 tested models, some of the models were abandoned based on their remaining usefulness to make new blank models (see Fig. 4 (a)). Ten new blank models were prepared in advance each day in case a target model cannot nest into any of the preserved models.

4.2 The setup of the HFFB procedure

4.2.1 Wind angle

Wind angle is another parameter that needs to be evaluated for wind design since the critical response can occur at any wind direction for high-rise buildings with different aerodynamic shapes (Lu et al., 2023). In theory, wind angle could be an input to the surrogate model, such as the literature using CFD simulation (Elshaer et al., 2017; Elshaer and Bitsuamlak, 2018), implying that there is no need to test all wind angles for a given shape. However, such an approach will lead to several problems for SB-CP-ASO procedure. First, models with the same shape may need to be retested at different times for different wind angles. Since it is impractical and impossible to preserve all models with limited space and resources, the same model may need to be remanufactured several times. Second, the demand of accuracy for surrogate modeling is increased since the objective function is pursuing the best performing model from the worst performing wind angle. Third, there is a fixed time to setup a model before data collection no matter how many wind angles are evaluated, including model installation, zeroing measurement devices, and initializing fan speeds (see Fig. 5 (b)). If the same model is tested at different times, the time to collect data will be significantly reduced.

For the aforementioned reasons, wind angle is taken as a testing condition and not as an input in the SB-CP-ASO procedure. An additional benefit to testing all wind angles is that the trend of the responses across different wind angles can be used to evaluate whether a response is an outlier or not (i.e., the responses should not differ significantly from the responses at adjacent wind angles) since the results of wind tunnel testing are nondeterministic. Note that the pros and cons of taking wind angle as a testing condition mentioned above do not apply for studies using CFD simulation, another critical difference between SB-ASO and SB-CP-ASO procedures.

4.2.2 Testing conditions

Since all models are doubly-symmetric, a total of 10 wind angles from 0° to 45° at 5-degree increments was used as a testing condition. To simulate the boundary layer effects, a suburban terrain condition with power-law index of 0.22 was generated in the test section with a length scale ratio of 1:750. The mean wind speed at model height was 9.8 m/s with a fan speed of 750 RPM (revolutions per minute). The approach flow conditions were evaluated in the longitudinal direction including: (1) mean wind speed profiles, (2) turbulence intensity profiles, and (3) PSD at the model height. More details of the approach flow conditions can be found in the literature (Lu et al., 2023). In addition, the aerodynamic performance of the benchmark model, SQ70, was evaluated in the testing condition before exploring the optimization problem using the SB-CP-ASO procedure. By doing this, the testing setup, including measurement devices, approach flow conditions, and model orientations can be validated with benchmark data.

To calculate the structural responses, the structural properties assumed for this study are summarized in Table 2. The full-scale building height and width were 300 m and 52.5 m, respectively. The fundamental frequency was assumed to be 0.1 Hz with a damping ratio of 1%. The building density was assumed as 200 kg/m^3. Linear mode shapes in the along and across wind direction were considered.

Table 2. Structural properties.

Parameters	Value
Building height, H_F	300 m
Building width, B_F	52.5 m
Fundamental frequency, f_1	0.1 Hz
Damping ratio, ξ	0.01
Mass per unit volume	200 kg/m^3

4.2.3 Aerodynamic response of the benchmark model

Fig. 14 (a) shows the variation of base moment coefficients for the benchmark model (SQ70) under different wind angles. The peak $\overline{CMD}$ (mean along-wind base moment coefficient) is 0.64 at the wind angle of 40°, and the peak σ_{CML} (standard deviation across-wind coefficient) is 0.15 at the wind angle of 0°. Fig. 14 (b) shows the PSD responses for the benchmark model in the across-wind direction under different wind angles. The responses are mainly dominated by the wind angle of 0° with the Strouhal number of 0.1. As wind angles larger than 20°, the amplification effects are negligible in comparison with the wind angle of 0°. Both the time and frequency domain results are consistent with the literature (Tamura and Miyagi, 1999; Tanaka et al., 2012; Carassale et al., 2014; Lu et al., 2023). Fig. 14 (c) shows the peak roof drift demands for the benchmark model for wind speeds of 40 m/s to 60 m/s. The drifts are controlled by the across-wind direction. The roof drift demands are larger than 2% and 3% at the wind speeds of 48 m/s and 53 m/s, respectively, suggesting the need to suppress wind responses through aerodynamic modification strategies.

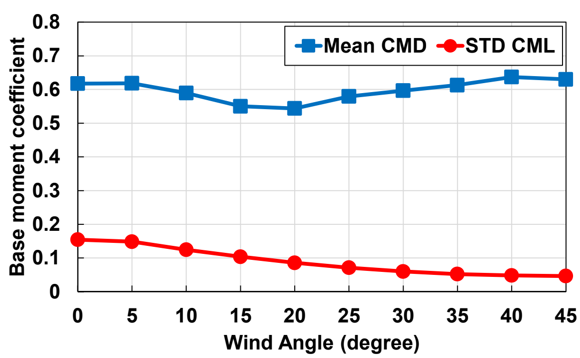

(a) Base moment coefficients

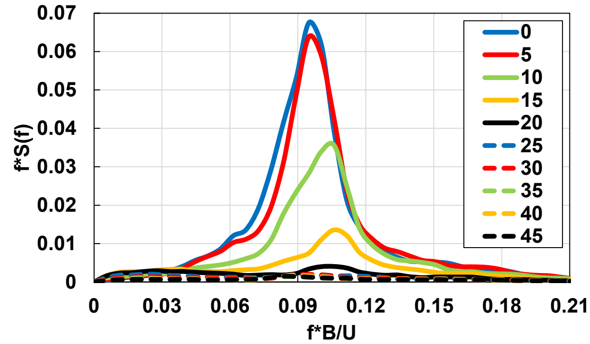

(b) PSD responses

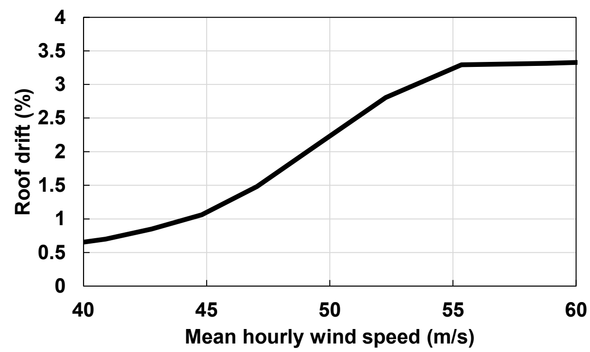

(c) Roof drift demands

Fig. 14. Wind tunnel testing results for the benchmark model

4.3 The setup of the infilling strategy

Based on the available BLWT testing window and the expected throughput of the SB-CP-ASO procedure, the first stop criterion was set as 200 iterations (specimens). Ten initial samples were selected using the Latin Hypercube Sampling technique (McKay et al., 1979). Three optimization objectives, mean along-wind coefficient ($\overline{CMD}$), RMS across-wind coefficient (RMS_{CML}), and standard deviation across-wind coefficient (σ_{CML}), were pursued in parallel in the optimization process. The $\overline{CMD}$, RMS_{CML}, and σ_{CML} refer to the maximum values across all wind angles. An independent ordinary kriging model using the Gaussian regression approach was generated for each of the objective functions using the ooDACE (Couckuyt et al., 2014) toolbox in MATLAB. As a proof-of-concept study, three objectives were selected to demonstrate that multiple objectives can be pursued in parallel. Note that when infilling for one of the three objectives, the accuracy of the surrogate model for all three objectives is improved. Alternatively, because σ_{CML} is critical to the wind response of tall buildings, it could have been pursued in isolation.

A fixed, equal ratio was used to alternate between infill goals of global exploration (Goal 1) and optimization (Goal 2). For global accuracy infilling, TOPSIS weights were selected as 0.5 for the sparsity level and 0.167 each for the predicted MSEs of the three optimization objectives. For optimization infilling, a fixed-sequence for the three objective functions was adopted, essentially converging them in parallel. With the three design variables (3D problem), the available search distances are 1-unit, 1.4-unit, and 1.7 unit- distances. The initial local search bound for the three objectives was select as 1.4-unit distance with the intention to demonstrate that a better solution can be achieved through a shortcut path. With two alternating infill goals and three alternating objectives, the infill pattern repeats every six iterations. If one objective is converged (the search bound is full), the optimization infilling will focus on other objectives instead (e.g., infill pattern repeats every four iterations). The local search bounds for the three objectives will be increased to 1.7 unit-distance at the same time until the optimal solutions are all converged if there is enough testing time remaining.

5. The optimization results of the SB-CP-ASO procedure

This section discusses the optimization results of the double-section setback problem through the SB-CP-ASO procedure. A total of 173 models were evaluated in 11 workdays. The three optimization objectives all converged with a search bound of 1.4-

unit distance. The reliability and the throughput of the adaptive subtractive manufacturing and HFFB testing procedures are discussed in Sections 5.1 and 5.2, respectively. The robustness of the infilling strategy is discussed in Sections 5.3 and 5.4 with respect to the input of samples and the convergence history of the three objective functions. A brief summary of the SB-CP-ASO procedure is presented in Section 5.5.

5.1 Evaluation of the adaptive subtractive manufacturing procedure

The reliability of the proposed adaptive subtractive manufacturing technique (introduced in Section 3.1) integrated into the SB-CP-ASO procedure is discussed in this subsection. The discussion includes model reusage, manufacturing time, and downtime in the iteration process.

5.1.1 Remanufacturing technique

Through the remanufacturing technique, 68 individual models were used to create the 173 models, indicating 60% foam material was saved. Fig. 15 shows the photos of preserved models at different days in the SB-CP-ASO procedure (note the models are displayed on foam stands of different heights). Fig. 16 shows the number of times the 68 individual models were reused. The individual models were reused an average of 2.54 times with a minimum of zero (not reused) and maximum of four.

(b) Day3 (31 models) (c) Day5 (37 models) (d) Day11 (40 models)

Fig. 15. Photographs of blank models and tested models.

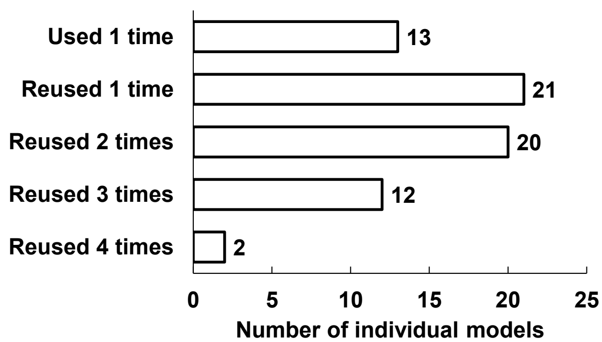

Fig. 16. Number of reused times for tested models.

5.1.2 Manufacturing time and downtime

Fig. 17 (a) shows the manufacturing time for the infilled samples along the iteration process (after collecting the results of initial samples). With the help of the adaptive milling procedure, the average manufacturing time for the 163 infilled candidates was 10 mins, which is considered as very fast for shape optimization problems with major modification strategy. The wind tunnel downtime for each iteration in the SB-CP-ASO procedure is presented in Fig. 17 (b). It can be seen that there is no downtime for 126 samples and the average downtime is 45 secs in the entire procedure. The downtime is defined as the time between the end of data collection for the previous model and the start of installation of the next model in the wind tunnel. The negligible downtime demonstrates the efficiency of the SB -ASO procedure is not influenced by model manufacturing, which is a critical challenge for SB-CP-ASO problems resolved by using the IIM&T technique.

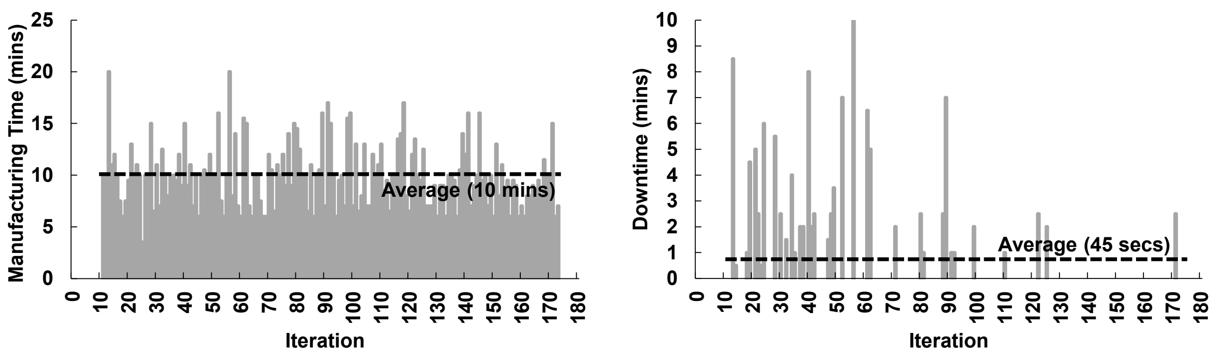

(a) Manufacturing time (b) Downtime

Fig. 17. The manufacturing time and downtime at each iteration in the ASO procedure.

The success of the IIM&T technique is attributed to the fast manufacturing time (10 mins on average, see Fig. 17 (a)), which is less than half of the HFFB testing procedure (25 mins on average, discussed later). It is worth repeating that the manufacturing process is preceded by analyzing wind tunnel results, updating the surrogate models, running the infill strategy, and generating an adaptive milling strategy (see Fig. 2 (b)), which adds approximately 10 minutes to the actual manufacturing time. If the IIM&T was not adopted, the downtime for each iteration would be around 20 mins at each iteration, meaning that half of the entire testing window was not be used for data collection.

5.2 The throughput of the HFFB procedure

Fig. 18 shows the number of samples tested each day. On the first day, only seven models were evaluated due to apparatus installation for the HFFB testing. On the last day, only 5 models were evaluated because of the stop criteria of objective functions. On average, 17 models were evaluated each day from Day 2 to Day 10. Since the downtime was negligible (see Section 5.1), the entire reserved testing window was used for HFFB testing. The average testing time for one model under 10 wind angles, including model un/installation, zeroing measurement devices, and reaching desired approaching flow conditions, was 25 mins for the procedure presented in Fig. 5 (b). This is considered as a high-throughput HFFB BLWT testing procedure.

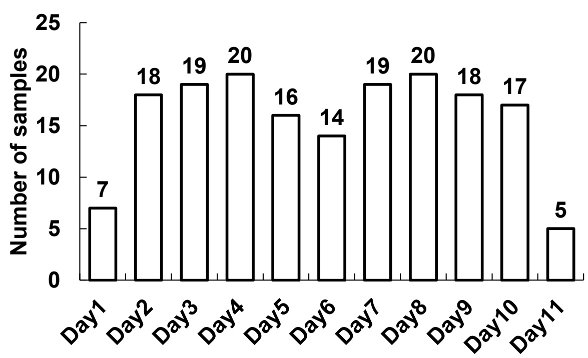

Fig. 18. Number of models tested each day.

5.3 The inputs of initial and infilling samples

The coordinates for the tested samples in the design space are presented in 3D and 2D plots in Fig. 19. Symbols are used to differentiate among initial samples, global exploration, optimum validation (Fig. 9 (a)), and local search (Fig. 9(b)). The optimal candidates for $\overline{CMD}$, RMS_{CML}, and σ_{CML} are (6,5,1), (6,10,4), and (6,7,4), respectively. Through the surrogate-based local search strategy, all samples are infilled within a 1.4-

unit distance around the optimal solutions. This local accuracy around optimal solutions can provide designers with more options without the concern of experimental uncertainties. In Fig. 19 (b)-(f), the success of the IIM&T technique realized through the sparsity level can be observed based on the fact that the samples for global exploration are shown to be well distributed and far from the local search areas even the outputs of the candidate tested in the wind tunnel were unknown.

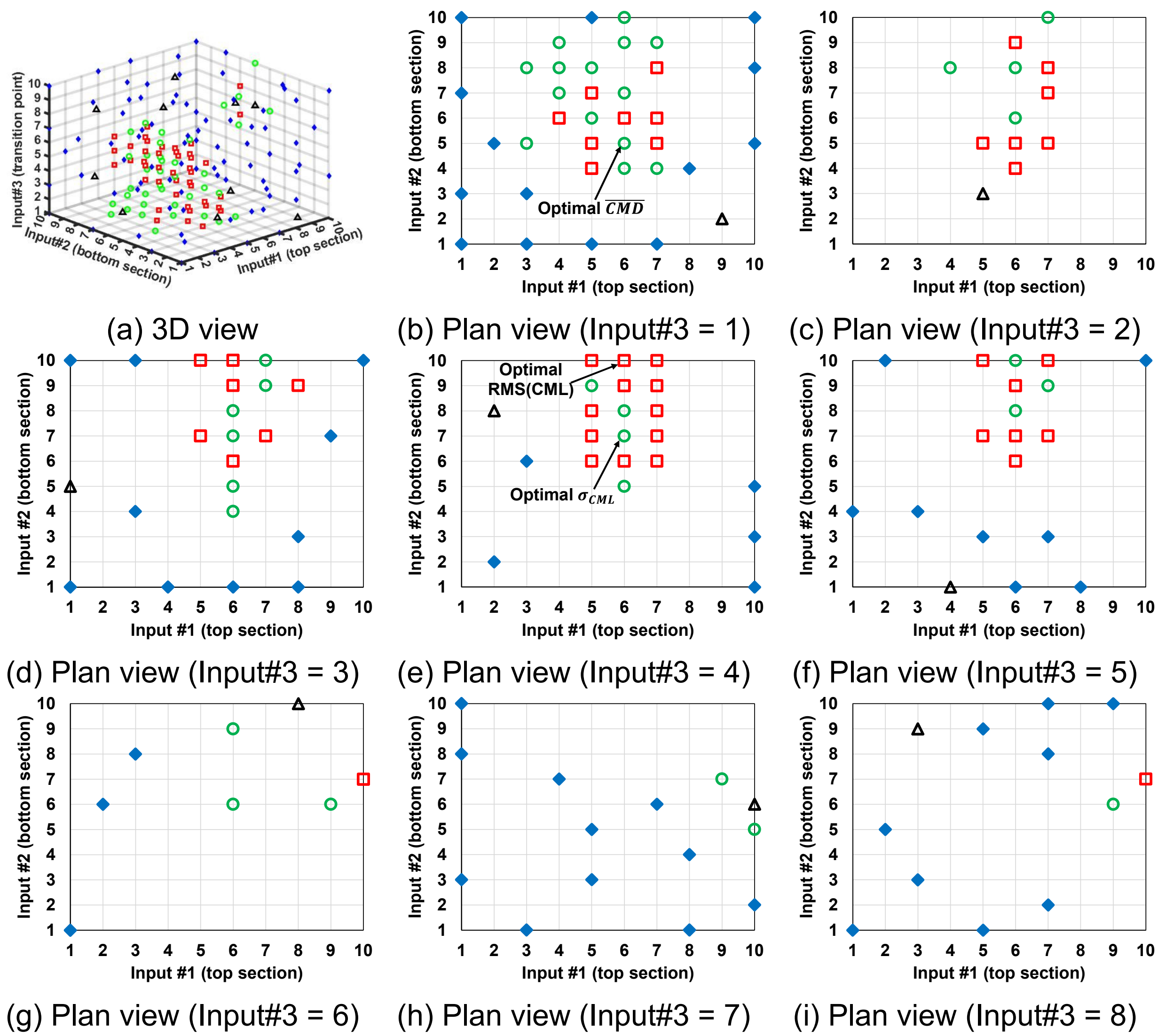

(a) 3D view
(b) Plan view (Input#3 = 1)
(c) Plan view (Input#3 = 2)
(d) Plan view (Input#3 = 3)
(e) Plan view (Input#3 = 4)
(f) Plan view (Input#3 = 5)
(g) Plan view (Input#3 = 6)
(h) Plan view (Input#3 = 7)
(i) Plan view (Input#3 = 8)

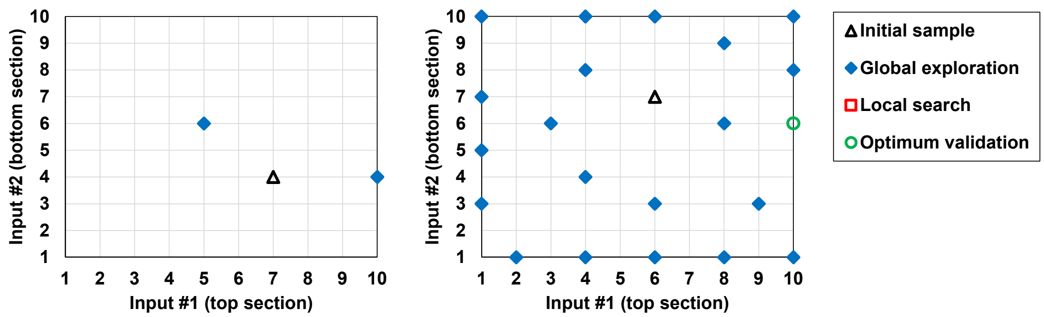

(j) Plan view (Input#3 = 9) (k) Plan view (Input#3 = 10)

Fig. 19. The coordinates for the initial samples and infilled samples.

Fig. 20 shows the ratio a given infill function was called and the locations on the domain where the infilling was made. With the fixed ratio between the two infill goals, it can be seen that 51% (82 samples) of total infilled samples are used for global exploration (Goal 1). Considering the infilling location, 18%, 16%, and 4% of total infilled samples are on the faces, on the edges, and at vertices, respectively. The results show that 76% of the samples for global exploration are infilled on the boundaries of the design space. The high infill ratio on the boundaries is attributed to kriging being an interpolation regression approach. The predicted MSEs on the boundaries are normally larger than that of in the domain if the distance between collected data points are the same. This indicates the weakness of the MSE-based infilling alone if important regions are not only the boundaries of a design space. For Goal 2 (optimization), 26% (43 samples) of total infilled samples are used for the surrogate-based local search and 23% (38 samples) are used for optimum validation. The similar infilling ratios for the two situations implies the mobility of the optimal solutions as the surrogate model increases in accuracy and the effectiveness of the jump-out mechanism from a local optimum solution.

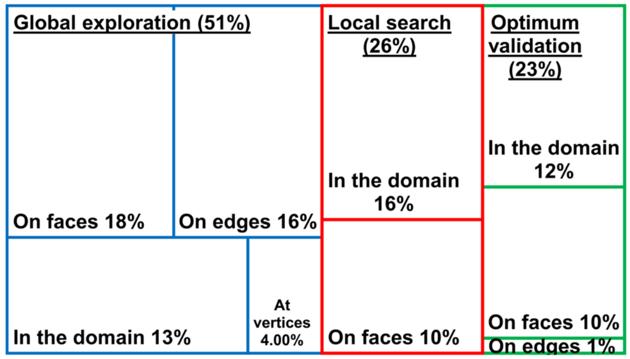

Fig. 20. The position for the infilled samples for different infill goals.

The sparsity level for different infill goals along the iteration process is shown in Fig. 21. The switch between the two infilling goals along the infilling process can be clearly seen. For global exploration, there are only 6 samples whose sparsity level is not 100%. This indicates that the samples are successfully infilled at spatially distributed coordinates to improve the global accuracy of surrogate modeling even without the results for the model tested in the wind tunnel. For optimization infilling, the sparsity levels decrease as the number of collected samples increases. Most of the infill candidates are used for optimization validation when the number of total samples is less than 35, meaning that the optimal solutions are not stable. After Iteration 60, more iterations are used for local search purpose, indicating that the local accuracy of promising regions is improving.

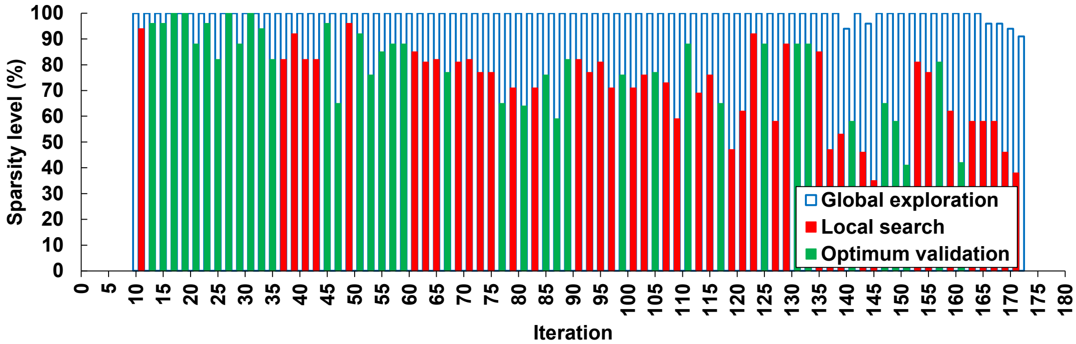

Fig. 21. Sparsity level at each iteration in the ASO procedure.

5.4 Convergence history of objective functions

This subsection discusses the convergence history for the optimization objectives of $\overline{CMD}$ (Fig. 22), RMS_{CML} (Fig. 23), and σ_{CML} (Fig. 24) along the iteration process. Fig. 22 (a), Fig. 23 (a), and Fig. 24 (a) show the convergence history of outputs, which are normalized by the first initial sample (3,9,8). Fig. 22 (b), Fig. 23 (b), and Fig. 24 (b) indicate the Euclidean distance of inputs (coordinates) between the current best solution and the final optimal solution. The observation line tracks the cumulative optimal solution, and the prediction line indicates the real-time optimal prediction by the surrogate model. With different purposes in the optimization process, the samples (inputs and outputs) for optimum validation are the same as the prediction from the surrogate model (Fig. 9 (a)), and the samples for local search are the same as observation (Fig. 9 (b)). The detailed information on the optimization history, including the coordinates of the infilling samples for surrogate-based local search or optimal validation, and the normalized cumulative optimal solution, is summarized in Table A1 ($\overline{CMD}$), Table A2 (RMS_{CML}), and Table A3 (σ_{CML}). As discussed in Section 3, the model (infilling sample) for n^{th+1}iteration is manufactured at n^{th} iteration and the outputs are obtained at n^{th+2} iteration in the IIM&T technique. In Table A1, for example, the model

(5,4,1) for local search purpose is manufactured at Iteration 11, tested in the wind tunnel at Iteration 12, and analyzed at Iteration 13. With the same concept in Fig. 22-24, the models are manufactured at iterations indicated by the points of local search and optimum validation, and the results are obtained after 2 iterations.

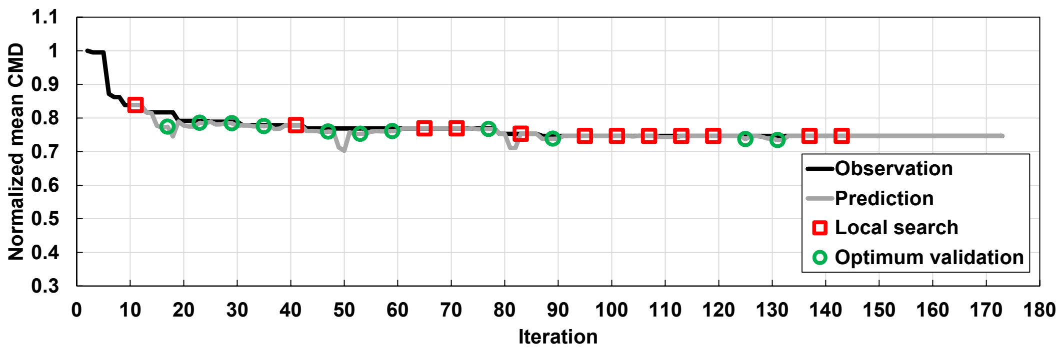

(a) Normalized $\overline{CMD}$

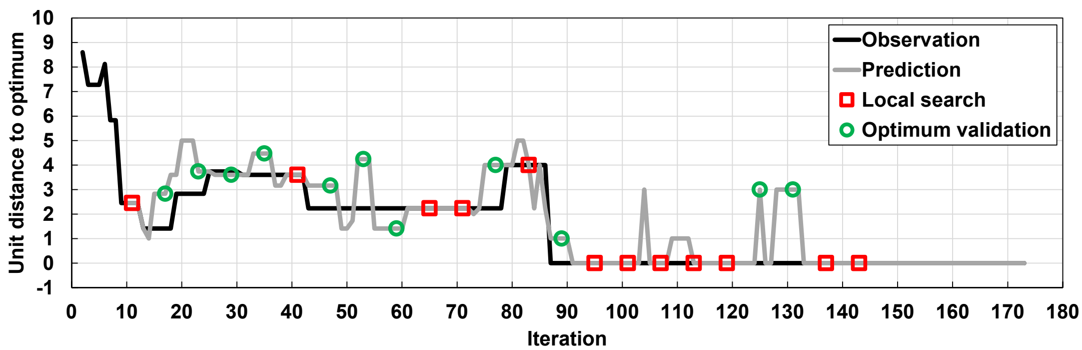

(b) The Euclidean distance between current optimum and final optimum

Fig. 22. The convergence history for $\overline{CMD}$.

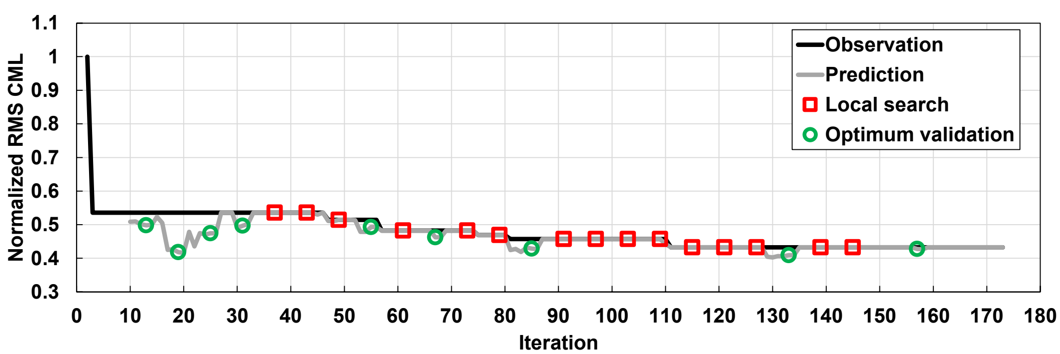

(a) Normalized RMS_{CML}

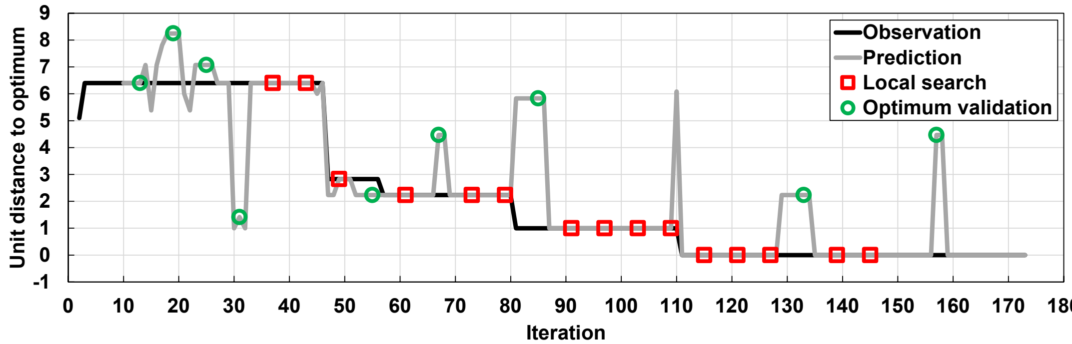

(b) The Euclidean distance between current optimum and final optimum
Fig. 23. The convergence history for RMS_{CML}.

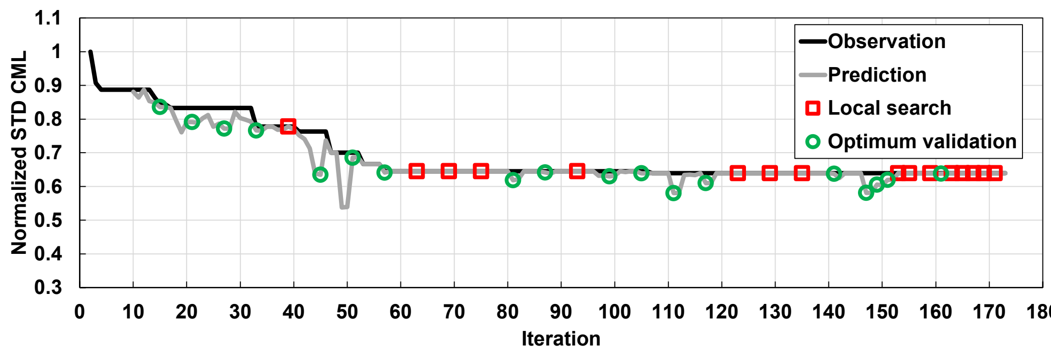

(a) Normalized σ_{CML}

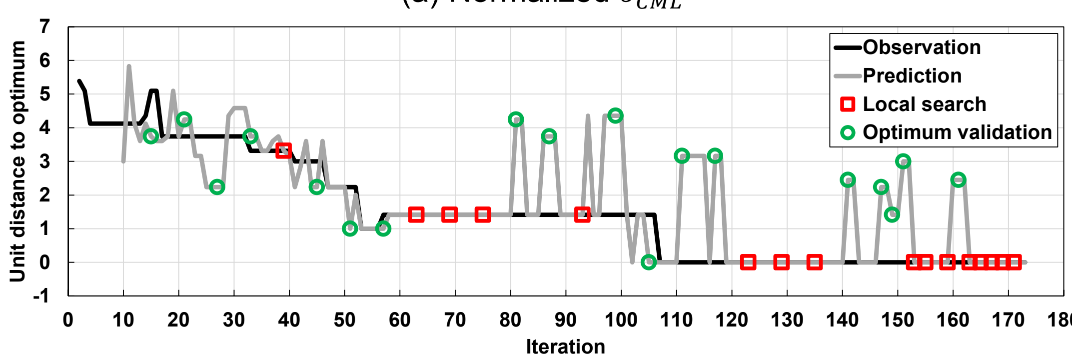

(b) The Euclidean distance between current optimum and final optimum
Fig. 24. The convergence history for σ_{CML}.

5.4.1 Mean along-wind responses

In Fig. 22, the optimum validation and surrogate-based local search for $\overline{CMD}$ are activated 11 and 12 times, respectively. By applying optimum validation, the predictions are proved to be only correct for 4 times. When the predictions are wrong, it can be observed that the predicted outputs are unconservative (see Fig. 22 (a)) and the corresponding inputs (see Fig. 22 (b)) are several unit-distances away from the cumulative optimal observation. The incorrect inputs will result in outputs which are not only worse than predictions but also than the cumulative optimal observation. This is a serious issue that should not be ignored for surrogate-based optimization studies, especially for real-world applications using physical testing. By switching between the two infilling goals, the issue is relieved immediately by conducting optimum validation without wasting more samples based on the incorrect predictions. In addition, valid optimal solutions are obtained anytime along the infilling process. In the end, the results from prediction and observation converge in both the inputs and outputs.

In comparison with the initial solution, the output of the final optimal $\overline{CMD}$ is reduced by 25.4% and the input is moved by 8.6-unit distance. The optimal solutions are improved 7 times (Iteration 13, 19, 25, 31, 43, 79, and 87) after collecting the results of initial samples. It is worth repeating that corresponding points for local search and optimum validation shown in Fig. 22 are manufactured at n-2 iterations. The 7 improvements are 4 times from optimum validation, 2 times from local search, and 1 time from other infilling purpose. This demonstrates that better solutions can come from different sources, reducing the chance of getting stuck at a local optimum solution. For optimum validation, the distances between the previous and improved solutions are 3.16-, 1.40-, 1.00-, and 2.24-unit distances at the iterations of 19, 25, 31, and 79, respectively. For Iteration 19 and 79, the moving distances are larger than that of the search bound (1.4-unit distance), showing the ability to find a better solution via the jump-out mechanism. For surrogate-based local search, optimal solutions are improved from 0.838 at (5,3,2) to 0.817 at (5,4,1) at Iteration 13, and from 0.778 at (4,8,1) to

0.769 at (5,7,1) at Iteration 43. The moving distances for the both improvements are all 1.4-unit distance, indicating the improved solutions are all led through the shortcut in the local search bound. The final optimal solution of $\overline{CMD}$ is at the coordinates of (6,5,1), which is resulted from the optimal validation of RMS_{CML} (see Table A2), showing the benefit of pursuing different objective functions in parallel. The optimization process for $\overline{CMD}$ halts at iteration of 145 because of the stop criterion for the local search strategy.

5.4.2 RMS across-wind responses

For RMS_{CML}, the local search and optimal validation are executed 15 times and 9 times, respectively, as shown in Fig. 23. The optimal solutions are improved 5 times (Iteration 47, 57, 75, 81, and 111) in the infilling process. In comparison with the initial solution, the output of the final optimal RMS_{CML} is reduced by 56.7% and the input is moved by 5.1-unit distance. The results suggest that the setback strategy is more effective in reducing across-wind responses than that of along-wind for high-rise buildings. The benefit of conducting parallel optimization objectives can be observed again at the iteration of 47, where the better solution is resulted from the optimum validation of σ_{CML}(see Table A2 and A3). The responses are decreased from 0.536 to 0.514 with a moving distance of 6.7-unit from the coordinates of (10,6,7) to (6,8,2). The need to apply optimal validation can be observed since the prediction of the surrogate model is only correct 1 time at Iteration 57, where the normalized $RMS_{CML}$is decreased from 0.514 at (6,8,2) to 0.482 at (6,8,3). When the kriging model makes incorrect predictions (8 out of 9 times), the discrepancies of the inputs (see Fig. 23 (b)) are more significant than that of $\overline{CMD}$. For example, the Euclidean distances between the prediction and observation at the iterations of 31 and 85 are 6.4- and 5.4-unit distances, respectively. In the 15 times of local search, the solutions are improved 3 times (Iteration 75, 81, and 111). The moving distances are 1.4-unit at the iterations of 75 and 81. At iteration of 111, the solution moves from the coordinates of (6,10,3) to (6,10,4) with a 1-unit distance, which is the final optimal solution for the objective of RMS_{CML}. At iteration of 147, the optimization procedure for RMS_{CML} is stopped because of the stop criterion of local search. The optimization process for RMS_{CML} is activated again at the Iteration 157 due to the prediction of better solution at the coordinates of (6,6,6). However, the prediction is proved to be wrong by conducting optimum validation at the iteration of 159 and the stop criterion is triggered again for RMS_{CML}.

5.4.3 STD across-wind responses

For σ_{CML}, the local search and optimal validation are executed 16 times and 18 times, respectively, as shown in Fig. 24. In comparison with the initial solution, the output of the final optimal is reduced by 36.1% and the input is moved by 5.4-unit distance. The optimal solutions are improved 9 times (Iteration 14, 15, 17, 33, 41, 47, 53, 57, and 107) in the infilling process. In addition to local search and optimum validation, the source of the improvements is also from global exploration, which is at Iteration 14 by infilling a data point at the coordinates of (5,10,1). There are 3 times (Iteration 14, 33, and 57) of improvements resulted from the optimization process of RMS_{CML}, indicating the correlation between the RMS_{CML} and σ_{CML} in the across-wind direction. The solution is improved 1 time by the local search at Iteration 41 with a moving distance of 1.4-unit distance. For optimum validation, when kriging makes an inaccurate prediction, the discrepancy of the inputs between the prediction and observation should not be ignored. The mobility of the incorrect predictions for σ_{CML} is more obvious than that of $\overline{CMD}$ and RMS_{CML}. In the 18 times of optimum validation, the solutions are improved 4 times at the iterations of 17, 47, 53, and 107 with the moving distances of 2-, 2.44-, 1.4-, and 1.4-unit distance, respectively. The final optimal solution is achieved at the iteration of 107. At the end of the infilling process, it can be observed that the frequency of the optimization process for σ_{CML} is increased after the iteration of 147. The reason behind this is because the optimization procedures for $\overline{CMD}$ and $RMS_{CML}$are stopped. Thus, the infill pattern repeats every 2 iterations between global exploration and optimization. At Iteration 173, the SB-CPASO procedure is stopped by the local search criterion of σ_{CML}.

5.5 Discussion

The optimization results of the double-section setback problem for high-rise buildings were discussed in this section. The reliability and efficiency of the manufacturing and testing components in the SB-CP-ASO were demonstrated with respect to model reusage and time. The effectiveness of the sparsity level was discussed through sample distributions. The robustness of the infilling strategy was evaluated through the convergence history of inputs and outputs for $\overline{CMD}$, RMS_{CML}, and σ_{CML}. For optimization purpose, the source of improved solutions comes from optimum validation, surrogate-based local search, or other infilling purposes (e.g., global exploration). The multiple sources of improvements reduce the chance of getting stuck at a local optimum.

A total of 173 samples/iterations were collected to reach the convergence criteria for the three optimization objectives with a local search bound of 1.4-unit. With the flexibility of the infilling strategy, the number of iterations can be reduced by the following: (1) decreasing the number of optimization objectives, (2) increasing the infilling ratio for the optimization goal, and (3) decreasing the radius of the local search bound if a shorter testing window was reserved. Because this was a proof-of-concept study, we selected three optimization objectives and a relaxed stopping criteria that allowed for the generation of a large aerodynamic database. Considering the diminishing returns after 60 iterations, an operator in a non-research setting may have elected to stop the process earlier. It is worth emphasizing that the benefits of the proposed infilling strategy, including (1) the validation optimum solution at any iteration, (2) the jump-out mechanism from local optimum, and (3) the local accuracy at important areas still exist with a shorter iteration process.

The size of design space (i.e., the number of parameters and their discretization) needs to be appropriate for the anticipated number of BLWT experiments. In this case, the design space has 1000 possibilities and the goal was to explore 10-20% through experimentation. The area around the optimal solution could be explored more thoroughly with a finer discretization at the cost of additional experimentation. However, there is also a practical lower bound on what resolution will produce an aerodynamic difference that is detectable above the experimental uncertainty.

6. Selection of candidates with promising structural response for high-rise buildings

This section presents a comparison approach for candidates with promising structural responses of high-rise buildings. The cumulative largest structural responses (enveloped over all wind angles and considering all wind speeds up to the design wind speed) was calculated for each of the 173 models obtained from Section 5. With this data, a convergence history of the best structural scale response at the design wind speed can be plotted versus iteration. More directly, the set of candidates which meet a given response threshold can be extracted for further consideration beyond aerodynamic performance. In addition to single design wind speed, it is suggested to consider multiple design wind speeds for different objectives at various hazard levels. Practical information of the double-section setback strategy is discussed based on the features of the promising candidates. The justification of using time domain results as the objective functions in the SB-CP-ASO procedure is discussed in the end.

6.1 Single design wind speed

Since aerodynamic strategies are more effective under high wind speeds for the mitigation of survivability (Lu et al., 2023), the roof drift responses for wind speeds of 40 m/s, 50 m/s, and 60 m/s, are used for selecting candidates with promising aerodynamic performance. The convergence history of the largest roof drift demands, all controlled by the across-wind direction, for the three design wind speeds are presented in Fig. 25. Note that responses do not necessarily monotonically increase with wind speed, so the cumulative largest response up to the design wind speed is used. The roof drifts of the benchmark model (SQ70, see Fig. 14 (c)) are also used for comparison. For the wind speed of 40m/s, the roof drifts for the benchmark, initial solution, and final optimal solution are 0.6%, 0.44%, and 0.29%, respectively. For 50m/s, these are 2.1%, 1.02%, and 0.51%, respectively. For 60m/s, they are 3.3%, 1.76%, and 0.63%, respectively. The greater reduction under the wind speeds of 50 m/s and 60 m/s suggests that the double-section setback strategy is more effective to mitigate roof drifts under higher wind speeds. The inputs of the final optima for the design wind speeds of 40 m/s, 50 m/s, and 60 m/s are (6,7,5), (6,10,3), and (6,9,2), respectively, demonstrating different design wind speeds do not have the same optimal solution.

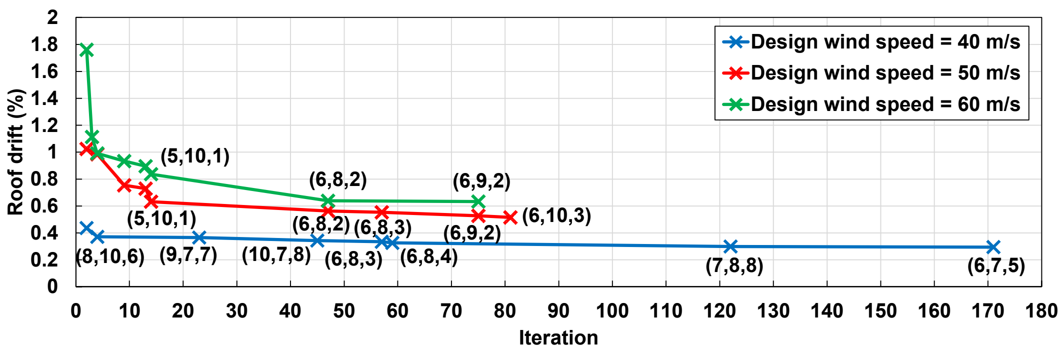

Fig. 25. The convergence history for roof drift demands with different design wind speeds.

Although the reductions of roof drifts are significant in comparison with the benchmark and initial solutions, in Fig. 25, it can be observed that the improvements are saturated at some point in the optimization process. For the design wind speed of 50 m/s, the improvements of roof drift demands are not significant after Iteration 47. By changing the external shapes from coordinates of (6,8,2), (6,8,3), (6,9,2), to (6,10,3), the roof drift demands are only improved by 5%. For 60 m/s, the roof drift demands are only improved by 1% after Iteration 47. Since the optimization process is continued until the stop criteria are triggered, there are other candidates (not pictured in Fig. 25) whose roof drift demands are similar but not better than that of the final optimal solutions.

These candidates should not be ignored for optimization problems of high-rise buildings since a set of candidates which can satisfy a defined threshold is needed for designers to achieve other objectives beyond aerodynamic performance (see the discussion in Section 2). With the convergence history of the response of interest, the threshold can be determined based on the saturation responses (in the absence of other guidance). In this study, the roof drift demands of 0.4%, 0.60%, and 0.75% are taken as the thresholds for the design wind speeds of 40 m/s, 50 m/s, and 60 m/s, respectively. In comparison with the benchmark model, the reductions of the thresholds of roof drift for the wind speeds of 40 m/s, 50 m/s, and 60 m/s are 34%, 72%, and 78%, respectively. For single design wind speed, there are 33 candidates, 13 candidates, and 12 candidates whose roof drift demands are below the thresholds of 40 m/s, 50 m/s, and 60 m/s, respectively.

6.2 Multiple design wind speeds

Fig. 26 presents promising candidates which can satisfy the defined thresholds for multiple design wind speeds (40 m/s, 50 m/s, and 60 m/s). The roof drifts for the minimum (1,1,1) and max (10,10,10) models in the design space are also included for comparison. The need to consider the cumulative largest response can be observed from the minimum model. The peak roof drift for (1,1,1) is 1.8% occurred at the wind speed of 45 m/s. If cumulative largest response up to the design wind speed is not considered, the roof drift for wind speeds higher than 45 m/s will be lower than 1.8% (e.g., 1.4% at the wind speed of 60 m/s), leading to unconservative design. The reason behind the non-monotonic increase in structural response is from variation of PSD responses caused by vortex shedding. The peak of PSD curves (or Strouhal number) occurs at different reduced frequencies for models with different external shapes. On the other hand, in comparison with (10,10,10), the results indicate that (1,1,1) is more promising for a single design wind speed at 60 m/s but is not as attractive for wind speeds lower than 53 m/s. This demonstrates again that optimal solutions vary with design wind speeds and hazard levels.

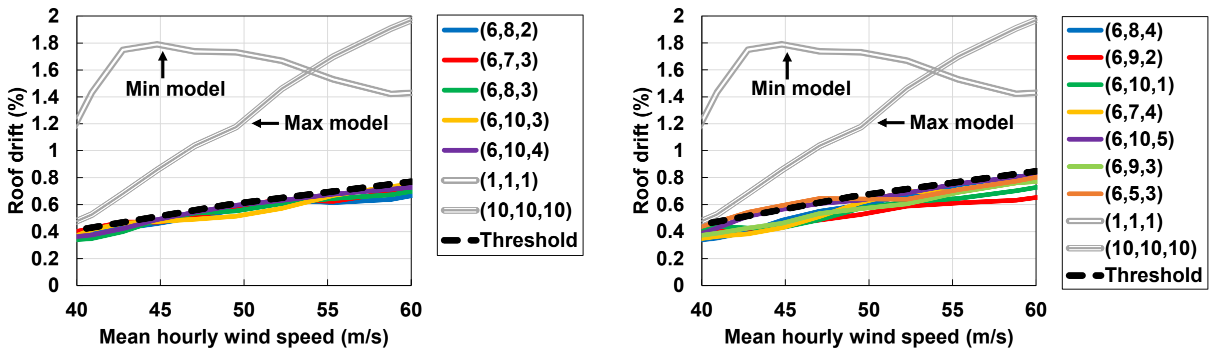

(a) Below the thresholds (b) Thresholds increased by 10%

Fig. 26. The roof drift demands for promising candidates considering multiple design wind speeds.

In line with performance-based design, the concept of multiple design wind speeds is suggested to select promising candidates which can achieve different thresholds at various wind speeds. In Fig. 26 (a), the thresholds for the three wind speeds are the same as discussed earlier. There are 5 promising candidates whose roof drift demands are below the thresholds. The photographs for the 5 promising candidates are presented in Fig. 27. The model volumes for the 5 promising candidates and the benchmark model are presented in Fig. 28. As mentioned in Section 4, the minimum and maximum model volumes in the optimization problem are 1397 cm^2 and 2930 cm^2, respectively. The building volumes for ideal candidates vary from 1938 cm^2 to

2230 cm^2, which do not occur at the extreme model volumes and are similar to the benchmark model (1960 cm^2). The results indicate that similar promising aerodynamic performance can be achieved with different building volumes. Also, the double-section setback strategy is a feasible option to significantly mitigate wind responses without the loss of building volume in comparison with the benchmark model.

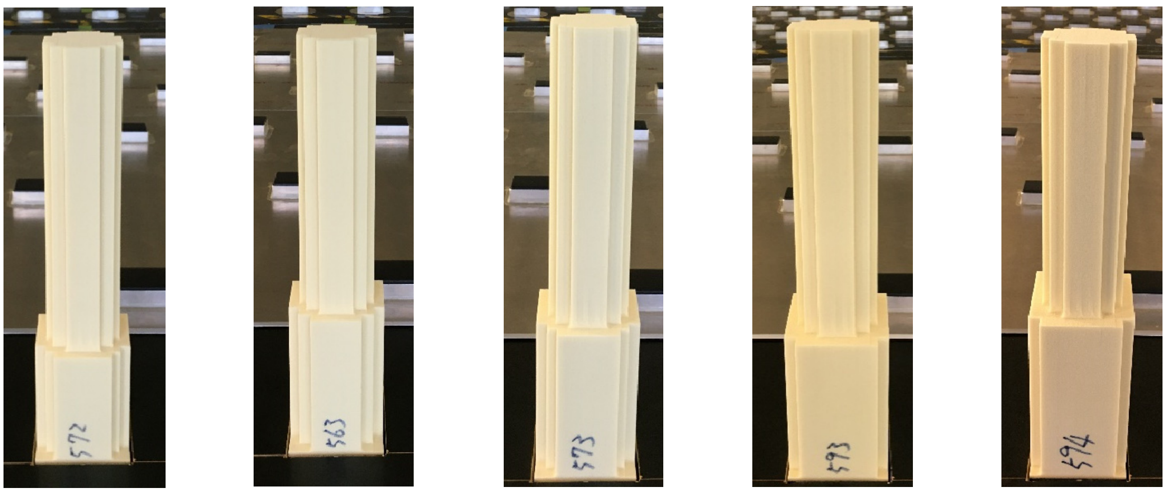

(a) (6,8,2) (b) (6,7,3) (c)(6,8,3) (d) (6,10,3) (e) (6,10,4)

Fig. 27. Photographs for candidates satisfied the thresholds of multiple design wind speeds.

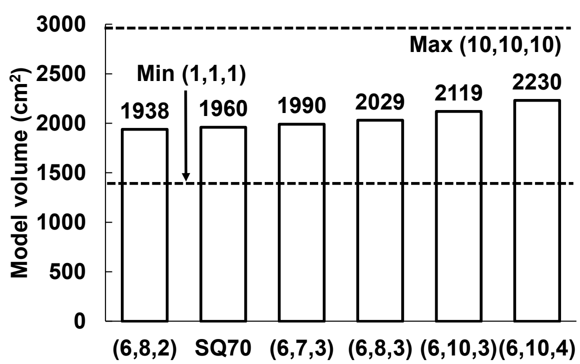

Fig. 28. Building volumes for the benchmark model (SQ70) and the candidates satisfied the thresholds of multiple design wind speeds.

In Fig. 26 (a) and Fig. 27, it can be observed that the 5 promising candidates are not intuitive but share consistent features. First, the inputs of the top section (input#1) are all the same, which is SQ56-7-31 (see Fig. 12, Option 6). The corresponding width ratio of the side protrusion is 55%. This indicates that a side protrusion with 55% width ratio and 12.5% depth ratio is a promising cross-section to reduce wind responses at higher part of high-rise buildings. The consistent results suggest that the 6 mm gap between options for the top section is large enough so that the results are not influenced by the uncertainties in the wind tunnel testing. Second, the ideal options for the bottom section (input#2) and transition positions (input#3) are within a bound. For the bottom section (Fig. 13), the ideal range is from Option 7 (SQ70-10-47) to Option 10 (SQ70-10-70). The corresponding width ratio is from 67% to 100%. The lower bound for the width of side protrusion for the bottom section (SQ-10-47) is still wider than that of the top section (SQ-56-7-31). For the transition position (Table 1), the ideal option varies from Option 2 (27.5% of model height) to Option 4 (42.5% of model height). The results suggest that the bottom section is less sensitive to the aerodynamic performance when the transition position is between 27.5% to 42.5% of the model height. The reason behind this is attributed to the boundary layer effects, where mean wind speed increases with elevation. In other words, the major aerodynamic responses, generated based on OTM, are not produced by the bottom section. Regarding the bound of the transient position, the results indicate the need to use sufficient length for both sections to destroy the coherence of vortex shedding effects at different elevations for the setback strategy.

The thresholds for multiple design wind speeds can be loosened if it is needed. By increasing the thresholds by 10% for the three wind speeds, 7 more candidates are obtained as shown in Fig. 26 (b). It can be observed that the inputs for the top section is consistent and the ranges of the bottom section and the transition position are increased. It should be emphasized that the candidates with similar promising responses presented in Fig. 26 are all collected observations, which can be used for discussion between owners, architects, and structural engineers in real-world applications without concerns about accuracy.

It is worthing noting that wind mitigation is decoupled from the early design stage of high-rise buildings for current design practice in the industry (Moorjani et al., 2021). Any changes on building shape or structural properties later in the design stage can be very expensive, time consuming, or even impossible. By applying the SB-CP-ASO procedure, a comprehensive optimization search can be carried out at the early design to avoid the aforementioned dilemma. Other design objectives, such as aesthetic appeal, building volume, and operation purposes, beyond aerodynamic performance can be applied to select the solutions obtained from the SB-CP-ASO, leading to a more efficient and economical design process. Additionally, solutions that are not selected become valuable candidates for future projects, building a large aerodynamic database.

Regarding the appropriateness of the objective functions pursued in the SB-CP-ASO procedure, it can be observed that the optimal solutions for RMS_{CML} (6, 10, 4) and σ_{CML} (6, 7, 4) in the time domain (discussed in Section 5) are included in Fig. 26. The results demonstrate that the time domain statistics with dynamic components in the across-wind direction are appropriate objective functions to find candidates with promising structural responses at multiple design wind speeds. This also implies that the number of iterations can be reduced by removing the objective function of $\overline{CMD}$, if a shorter wind tunnel testing window was reserved for the SB-CP-ASO procedure.

7. Conclusions

This study proposes a surrogate-based cyber-physical aerodynamic shape optimization (SB-CP-ASO) procedure for high-rise buildings under wind loading. The procedure consists of (1) an adaptive subtractive manufacturing technique, (2) a high-throughput high-frequency base balance (HFFB) wind tunnel testing, and (3) a highly flexible infilling strategy. A parallel manufacturing and testing (llM&T) technique is realized through an indicator, sparsity level, to ensure the efficiency of the SB-CP-ASO procedure. An unexplored double-section setback strategy with different cross-sections and transitions positions is used to demonstrate the performance of the three components in the procedure. Three objective functions in time domain were pursued in parallel in the online optimization process. A total of 173 samples were evaluated in 11 workdays and ended by the stop criteria for optimization convergence. As a proof-of-concept study, three objective functions and a relaxed stopping criteria were used, allowing for the generation of a large aerodynamic database.

The manufacturing speed and testing throughput were discussed. For the infilling strategy, a switch with a user-defined ratio between global exploration and optimization is suggested to (1) provide valid optimal solutions anytime along the iteration, and (2) build a jump-out mechanism from local optimum solution. In the optimization process, the infilling strategy is able to pursue multiple objective functions in parallel. A surrogate-based local search strategy with user-defined search bound is developed in the optimization process to (1) provide a flexible stop criterion controlled by users, (2) enhance the optimization performance, and (3) improve the local accuracy at promising regions, which can eliminate the concern of experimental uncertainties and provide more options for designers with considerations beyond aerodynamic behavior. Based on limited testing time, the convergence speed of the infilling process can be increased by adjusting (1) the infilling ratio between global exploration and optimization, (2) the number of objective functions, and (3) the radius of the local search bound without the loss of the aforementioned features.

The consideration of multiple design wind speeds is suggested to select promising candidates with structural responses below defined thresholds. Based on the convergence history of roof drift, the thresholds for wind speeds of 40 m/s, 50 m/s, and 60 m/s are 34%, 72%, and 78% lower than that of the benchmark model, indicating the effectiveness of the double-section setback strategy for high-rise buildings. The inputs for the promising candidates share consistent trends. For the top section, the same 55% width ratio of the side protrusion (SQ-56-7-31) is suggested for all ideal candidates. For the bottom section, the ideal option varies between 67% (SQ70-10-47) to 100% (SQ70-10-70) width ratios of the side protrusion. To effectively disturb the coherence of vortex shedding in the across-wind direction, the ideal transition position varies from 27.5% to 42.5% of the entire height.

This study presents comprehensive details regarding how to integrate CNC manufacturing, wind tunnel testing, and adaptive surrogate modeling technique in an online optimization problem with practical considerations to select promising candidates for high-rise buildings. The procedure is expected to provide an efficient platform between owners, architects, and structural engineers to find promising candidates within a design space for real-world applications. In addition, the three components developed in this study can be individually applied to different fields with further applications.

CRediT authorship contribution statement

Wei-Ting Lu: Conceptualization, Methodology, Investigation, Data Curation, Visualization, Validation, Writing - Original Draft. Brian M. Phillips: Conceptualization, Methodology, Project administration, Supervision, Validation, Writing - Review & Editing. Zhaoshuo Jiang: Conceptualization, Project administration, Writing - Review & Editing

Declaration of competing interest

The authors declare that they have no known competing financial interests or personal relationships that could have appeared to influence the work reported in this paper.

Acknowledgments

This material is based upon work supported by the National Science Foundation (NSF) under Grants No. 2028762 & 2028647. Any opinions, findings, and conclusions or recommendations expressed in this material are those of the authors and do not necessarily reflect the views of NSF. The authors also acknowledge the NSF NHERI awardee that contributed to the research results reported within this paper under Grant

No. 2037725: Natural Hazards Engineering Research Infrastructure: Experimental Facility with Boundary Layer Wind Tunnel 2021-2025 and Grant No. 2022469: Natural Hazards Engineering Research Infrastructure: Cyberinfrastructure (DesignSafe) 2020-2025.

Appendix A. Detailed converged history of objective functions

Table A1. Detailed convergence history of $\overline{CMD}$.

Iteration	Updated optimum		Infilling sample	
	Observation	Sample	Local search	Optimal validation
2	1.00	(3,9,8)	-	-
3	0.995	(10,6,7)	-	-
6	0.871	(7,4,9)	-	-
7	0.862	(2,8,4)	-	-
9	0.838	(5,3,2)	-	-
11	-	-	(5,4,1)	-
13*	0.817	(5,4,1)	-	-
17	-	-	-	(4,7,1)
19**	0.791	(4,7,1)	-	-
23	-	-	-	(4,8,2)
25**	0.789	(4,8,2)	-	-
29		-	-	(4,8,1)
31**	0.778	(4,8,1)	-	-
35	-	-	-	(4,9,1)
41	-	-	(5,7,1)	-
43*	0.769	(5,7,1)	-	-
47	-	-	-	(5,8,1)
53	-	-	-	(3,8,1)
59	-	-	-	(5,6,1)
65	-	-	(6,6,1)	-
71	-	-	(4,6,1)	-
77	-	-	-	(6,9,1)
79**	0.753	(6,9,1)	-	-
83	-	-	(7,8,1)	-
87^	0.746	(6,5,1)	-	-
89	-	-	-	(6,4,1)
95	-	-	(7,5,2)	-
101	-	-	(7,6,1)	-
107	-	-	(5,5,2)	-
113	-	-	(6,4,2)	-
119	-	-	(7,5,1)	-
125	-	-	-	(3,5,1)
131	-	-	-	(6,5,4)
137	-	-	(5,5,1)	-
143	-	-	(6,5,2)	-

"*" denotes the improved solution is resulted from local search
"**" denotes the improved solution is resulted from optimal validation
"^" denotes the improved solution is resulted from global exploration or other objective function

Table A2. Detailed convergence history of RMS_{CML}.

Iteration	Updated optimum		Infilling sample	
	Observation	Sample	Local search	Optimal validation
2	1.000	(3,9,8)	-	-
3	0.536	(10,6,7)	-	-
13	-	-	-	(9,6,8)
19	-	-	-	(10,6,10)
25	-	-	-	(10,5,7)
31	-	-	-	(7,10,3)
37	-	-	(10,7,6)	-
43	-	-	(10,7,8)	-
47^	0.514	(6,8,2)	-	-
49	-	-	(7,7,2)	-
55	-	-	-	(6,8,3)
57**	0.482	(6,8,3)	-	-
61	-	-	(7,8,4)	-
67	-	-	-	(6,6,2)
73	-	-	(6,9,2)	-
75*	0.469	(6,9,2)	-	-
79	-	-	(6,10,3)	-
81*	0.457	(6,10,3)	-	-
85	-	-	-	(6,5,1)
91	-	-	(5,10,4)	-
97	-	-	(5,10,3)	-
103	-	-	(7,10,4)	-
109	-	-	(6,10,4)	-
111*	0.433	(6,10,4)	-	-
115	-	-	(5,10,5)	-
121	-	-	(7,9,4)	-
127	-	-	(6,9,5)	-
133	-	-	-	(6,9,6)
139	-	-	(7,10,5)	-
145	-	-	(6,9,3)	-
157	-	-	-	(6,6,6)

"*" denotes the improved solution is resulted from local search
"**" denotes the improved solution is resulted from optimal validation
"^" denotes the improved solution is resulted from global exploration or other objective function

Table A3. Detailed convergence history of σ_{CML}.

Iteration	Updated optimum		Infilling sample	
	Observation	Sample	Local search	Optimal validation
2	1.000	(3,9,8)	-	-

3	0.907	(10,6,7)	-	-
4	0.887	(8,10,6)	-	-
14^	0.864	(5,10,1)	-	-
15^	0.844	(9,6,8)	-	(9,6,6)
17**	0.833	(9,6,6)	-	-
21	-	-	-	(9,7,7)
27	-	-	-	(5,9,4)
33^	0.778	(7,10,3)	-	(7,10,2)
39	-	-	(8,9,3)	-
41*	0.763	(8,9,3)	-	-
45	-	-	-	(6,8,2)
47**	0.700	(6,8,2)	-	-
51	-	-	-	(6,7,3)
53**	0.666	(6,7,3)	-	-
57^	0.645	(6,8,3)	-	(6,8,4)
63	-	-	(5,7,3)	-
69	-	-	(6,9,4)	-
75	-	-	(7,8,2)	-
81	-	-	-	(6,10,1)
87	-	-	-	(7,9,1)
93	-	-	(5,8,4)	-
99	-	-	-	(7,4,1)
105	-	-	-	(6,7,4)
107**	0.639	(6,7,4)	-	-
111	-	-	-	(6,4,3)
117	-	-	-	(6,10,5)
123	-	-	(7,6,4)	-
129	-	-	(5,6,4)	-
135	-	-	(7,7,5)	-
141	-	-	-	(7,9,5)
147	-	-	-	(6,5,3)
149	-	-	-	(6,8,5)
151	-	-	-	(6,7,1)
153	-	-	(5,7,5)	-
155	-	-	(6,6,5)	-
159	-	-	(7,7,3)	-
161	-	-	-	(7,9,3)
163	-	-	(6,6,4)	-
165	-	-	(5,7,4)	-
167	-	-	(7,7,4)	-
169	-	-	(6,7,5)	-
171	-	-	(6,6,3)	-

“*” denotes the improved solution is resulted from local search
“**” denotes the improved solution is resulted from optimal validation
“^” denotes the improved solution is resulted from global exploration or other objective function

References

Ahmed, M.Y.M., Qin, N., 2009. Surrogate-based aerodynamic design optimization: use of surrogates in aerodynamic design optimization. The 13th International

Conference on Aerospace Science and Aviation Technology. Military Technical College, Kobry Elkobbah, Cairo, Egypt.

ASCE 7-22, 2022. Minimum design loads and associated criteria for buildings and other structures. American Society of Civil Engineers, Reston, VA.

Bernardini, E., Spence, S.M.J., Wei, D., Kareem, A., 2015. Aerodynamic shape optimization of civil structures: A CFD-enabled Kriging-based approach. Journal of Wind Engineering and Industrial Aerodynamics. 144, 154-164.

Carassale, L., Freda, A., Marre-Brunenghi, M., 2014. Experimental investigation on the aerodynamic behavior of square cylinders with rounded corners. Journal of Fluids and Structures. 44, 195–204.

Catarelli, R.A., Fernández-Cabán, P.L., Masters, F.J., Bridge, J.A., Gurley, K.R., Matyas, C.J., 2020a. Automated terrain generation for precise atmospheric boundary layer simulation in the wind tunnel. Journal of Wind Engineering and Industrial Aerodynamics. 207, 104276.

Catarelli, R.A., Fernández-Cabán, P.L., Phillips, B.M., Bridge, J.A., Masters, F.J., Gurley, K.R., and Prevatt, D.O., 2020b. Automation and new capabilities in the University of Florida NHERI boundary layer wind tunnel. Frontiers in Built Environment. 6.

Chen, Z., Huang, H., Xu, Y., Tse, K.T., Kim, B., Wang, Y., 2021. Unsteady aerodynamics on a tapered prism under forced excitation. Engineering Structures. 240, 112387.

Couckuyt, I., Dhaene, T., Demeester, P., 2014. ooDace Toolbox: a flexible object-oriented kriging implementation. Journal of Machine Learning Research. 15, 3183-3186.

Ding, F., Kareem, A., 2018. A multi-fidelity shape optimization via surrogate modeling for civil structures. Journal of Wind Engineering and Industrial Aerodynamics. 178, 49-56.

Elshaer, A., Bitsuamlak, G., 2018. Multiobjective aerodynamic optimization of tall building openings for wind-induced load reduction. Journal of Structural Engineering. 144(10), 04018198.

Elshaer, A., Bitsuamlak, G., Damatty, A.E., 2017. Enhancing wind performance of tall buildings using corner aerodynamic optimization. Engineering Structures. 136, 133-148.

Fernández-Cabán, P.L., Whiteman, M.L., Phillips, B.M., Masters, F.J., Davis,J.R., Bridge, J.A., 2020. Cyber-physical design and optimization of tall building dynamics using aeroelastic wind tunnel modeling. Journal of Wind Engineering and Industrial Aerodynamics. 198, 104092.

Forrester, A.I.J., Keane A.J., 2009. Recent advances in surrogate-based optimization. Progress in Aerospace Sciences. 45(1–3), 50–79.

Gu, M., Quan, Y., 2004. Across-wind loads of typical tall buildings. Journal of Wind Engineering and Industrial Aerodynamics. 92 (13), 1147–1165.

Gu, M., Wang, X., Quan, Y., 2020. Wind tunnel test study on effects of chamfered corners on the aerodynamic characteristics of 2D rectangular prisms. Journal of Wind Engineering and Industrial Aerodynamics. 204, 104305.

Hwang, C.L., Lai, Y.J., Liu, T.Y., 1993. A new approach for multiple objective decision making. Computers and Operational Research. 20 (8), 889–899.

Hwang, C.L., Yoon K.,1981. Multiple attribute decision making: methods and applications: a state-of-the-art survey. New York: Springer-Verlag.
Irwin, P.A., 2009. Wind engineering challenges of the new generation of super-tall buildings. Journal of Wind Engineering and Industrial Aerodynamics. 97(7-8), 328–334.
Jones, D.R., Schonlau, M., Welch, W.J., 1998. Efficient global optimization of expensive black-box functions. Journal of Global Optimization. 13(4), 455–492.
Kareem, A., 1983. Mitigation of wind induced motion of tall buildings. Journal of Wind Engineering and Industrial Aerodynamics. 11(1-3) 273–284.
Kawai, H., 1998. Effect of corner modifications on aeroelastic instabilities of tall buildings. Journal of Wind Engineering and Industrial Aerodynamics. 74-76, 719–729.
Kim, Y., Kanda, J., 2010. Characteristics of aerodynamic forces and pressures on square plan buildings with height variations. Journal of Wind Engineering and Industrial Aerodynamics. 98 (8–9), 449–465.
Kim, Y., Kanda, J., 2013. Wind pressures on tapered and set-back tall buildings. Journal of Fluids and Structures. 39, 306–321.
Kim, Y., Kanda, J., Tamura, Y., 2011. Wind-induced coupled motion of tall buildings with varying square plan with height. Journal of Wind Engineering and Industrial Aerodynamics. 99 (5), 638–650.
Krige, D.G., 1951. A statistical approach to some basic mine valuations problems on the Witwatersrand. Journal of The Chemical Metallurgical and Mining Society of South Africa. 52(6):119–139.
Kwok, K.C.S., Wilhelm, P.A., Wilkie, B.G., 1988. Effect of edge configuration on wind-induced responses of tall buildings. Engineering Structures. 10(2), 135-140.
Kwon, D.K., Kijewski, T., Kareem, A., 2008. E-analysis of high-rise buildings subjected to wind loads. Journal of Structural Engineering. 134(7), 1139-1153.
Li, Y., Li, C., Li, Q.S., Song, Q., Huang, X., Li, Y.G., 2020. Aerodynamic performance of CAARC standard tall building model by various corner chamfers. Journal of Wind Engineering and Industrial Aerodynamics. 202, 104197.
Li, Y., Song, Q., Li, C., Huang, X., Zhang, Y., 2022. Reduction of wind loads on rectangular tall buildings with different taper ratios. Journal of Building Engineering. 45, 103588.
Li, Y.G., Yan, J.H., Li, Y., Xiao, C.X., Ma, J.X., 2021. Wind tunnel study of wind effects on 90° helical and square tall buildings: A comparative study. Journal of Building Engineering. 42, 103068.
Lu, W.T., Phillips, B.M., Jiang, Z., 2023. Effects of side and corner modification on the aerodynamic behavior of high-rise buildings considering serviceability and survivability. Journal of Wind Engineering and Industrial Aerodynamics. 233, 105324.
Matheron, G., 1963. Principles of geostatistics. Economic Geology. 58(8), 1246–1266.
McKay, M.D., Bechman, R.J., Conover, W.J., 1979. A comparison of three methods for selecting values of input variables in the analysis of output from a computer code. Technometrics. 21(2), 239–245.

Moorjani, R. R., Lombardo, F.T., Devin, A.F., Young, B.S., Baker, W.F., Ray, S.D., 2021. Influence of vented floors on the across-wind response of tall buildings. Journal of Wind Engineering and Industrial Aerodynamics. 209, 104480.

Paul, R., Dalui, S.K., 2021. Optimization of alongwind and crosswind force coefficients on a tall building with horizontal limbs using surrogate modeling. The Structural Design of Tall and Special Buildings. 30(4), e1830.

Qiu, Y., Yu, R., San, B., Li, J., 2022. Aerodynamic shape optimization of large-span coal sheds for wind-induced effect mitigation using surrogate models. Engineering Structures. 253, 113818.

Sacks, J., Welch, W.J., Mitchell, T.J., Wynn, H.P., 1989. Design and Analysis of Computer Experiments. Statistical Science. 4(4), 409-423.

Stathopoulos, T., 1985. Wind environmental conditions around tall buildings with chamfered corners. Journal of Wind Engineering and Industrial Aerodynamics. 21, 71-87.

Tamura, T., Miyagi, T., 1999. The effect of turbulence on aerodynamic forces on a square cylinder with various corner shapes. Journal of Wind Engineering and Industrial Aerodynamics. 83, 135–145.

Tanaka, H., Tamura, Y., Ohtake, K., Nakai, M., Kim, Y.C., 2012. Experimental investigation of aerodynamic forces and wind pressures acting on tall buildings with various unconventional configurations. Journal of Wind Engineering and Industrial Aerodynamics. 107–108, 179–191.

Townsend, J.F., Wang, J., Teschner, T.R., Xu, G., 2023. Towards an optimized design for an elevated cyclonic home using numerical simulations and active learning framework. Journal of Wind Engineering and Industrial Aerodynamics. 239, 105445.

Tschanz, T., Davenport, A.G., 1983. The base balance technique for the determination of dynamic wind loads. Journal of Wind Engineering and Industrial Aerodynamics. 13 (1-3), 429–439.

Tse, K.T., Hitchcock, P.A., Kwok, K.C., Thepmongkorn, S., Chan, C.M., 2009. Economic perspectives of aerodynamic treatments of square tall buildings. Journal of Wind Engineering and Industrial Aerodynamics. 97 (9–10), 455–467.

Wang, Z., Zheng, C., Mulyanto, J.A., Wu, Y., 2022. Aerodynamic Shape Optimization of a Square Cylinder with Multi-Parameter Corner Recession Modifications. Atmosphere. 13, 1782.

Wang, Z., Mulyanto, J.A., Zheng, C., Wu, Y., 2023. Research on a surrogate model updating-based efficient multi-objective optimization framework for supertall buildings. Journal of Building Engineering. 45, 106702.

Whiteman, M.L., Fernández-Cabán, P.L., Phillips, B.M., Masters, F.J., Bridge, J.A., Davis, J.R., 2018. Multi-objective optimal design of a building envelope and structural system using cyber-physical modeling in a wind tunnel. Frontiers in Built Environment. 22.

Whiteman, M.L., Fernández-Cabán, P.L., Phillips, B.M., Masters, F.J., Davis,J.R., Bridge, J.A., 2022. Cyber-physical aerodynamic shape optimization of a tall building in a wind tunnel using an active fin system. Journal of Wind Engineering and Industrial Aerodynamics. 220, 104835.

Xu, G., Kareem, A., Shen, L., 2020. Surrogate modeling with sequential updating: applications to bridge deck–wave and bridge deck–wind interactions. Journal of Computing in Civil Engineering. 34(4), 04020023.
Yoon, K., 1987. A reconciliation among discrete compromise situations. The Journal of the Operational Research Society. 38 (3), 277–286.
Zhou, Y., Kijewski, T., Kareem, A., 2003. Aerodynamic loads on tall buildings: interactive database. Journal of Structural Engineering. 129(3), 394-404.